

Supplementary Information

**Highly Near-IR-Emissive Ytterbium(III) Complexes with
Unprecedented Quantum Yields**

Ji-Yun Hu¹, Yingying Ning¹, Yin-Shan Meng¹, Jing Zhang², Zhuo-Yan Wu¹, Song
Gao^{1*} and Jun-Long Zhang^{1*}

¹Beijing National Laboratory for Molecular Sciences, State Key Laboratory of Rare
Earth Materials Chemistry and Applications, College of Chemistry and Molecular
Engineering, Peking University, Beijing 100871, P. R. China

²Beijing National Laboratory for Molecular Sciences, Institute of Chemistry, Chinese
Academy of Sciences, Beijing 100190, P. R. China

Correspondence should be addressed to J.-L. Zhang (Email:
zhangjunlong@pku.edu.cn) and S. Gao (email: gaosong@pku.edu.cn).

Table of contents

1. General.....	6
2. Synthesis.....	6
2.1 Porphyrins and Kläui's ligand.....	6
2.2 Porphyrinate lanthanide complexes.....	6
2.3 Summary of Crystallographic Data.....	11
2.4 NMR spectra.....	15
2.5 HR-ESI-MS spectra.....	25
2.6 IR spectra.....	33
3. Photophysical properties.....	36
3.1 General.....	36
3.2 Absorption, excitation and steady-state emission spectra.....	38
3.3 Luminescence decay profiles.....	43
3.4 NIR quantum yield measurement.....	49
3.4.1 Results via FLS 920 – Comparative Method.....	49
3.4.2 Results <i>via</i> FLS 920 – Integrating Sphere.....	50
3.4.3 Results <i>via</i> Fluorolog-3 spectrofluorimeter.....	52
3.5 Calculation of the quenching rate difference Δk	53
3.6 Radiative luminescence lifetime τ_{rad} measurement.....	54
4. References.....	55

1. General

UV/Vis spectra were recorded on an Agilent 8453 UV/Vis spectrometer equipped with an Agilent 89090A thermostat (0.18°C). Near-IR absorption spectra were recorded on a SHIMADZU UV3600PLUS spectrometer. Mass spectra were recorded on Bruker APEX IV FT-ICR mass spectrometer (ESI-MS) Elemental analyses (C, H, N) were recorded on Elementar Analysensysteme GmbH vario EL Elemental Analyzer. NMR spectra were recorded on a Varian Mercury Plus 300 MHz spectrophotometer or Bruker ARX400 400MHz spectrophotometer. IR spectra were recorded on a Bruker VECTOR22 FTIR spectrometer as KBr pellets. Intensity data for crystals were collected on a Bruker Smart Apex II CCD diffractometer with graphite-monochromated Mo K α radiation (0.71073 Å) at 180 K or 277 K. The structures were solved by direct methods and refined with the full-matrix least-squares technique based on F^2 using the SHELXL program. All non-hydrogen atoms were refined anisotropically. Hydrogen atoms were placed at the calculation positions. Emission spectra and lifetime measurements were recorded on an Edinburgh Analytical Instruments FLS920 lifetime and steady-state spectrometer (450 W Xe lamp/microsecond flash lamp, PMT R928 for visible emission spectrum; Hamamatsu R5509-73 PMT with C9940-02 cooler for NIR emission spectrum,).

CH₂Cl₂ was distilled from calcium hydride. CD₂Cl₂ (99.8% D) was purchased from Cambridge Isotope Laboratories, Inc. and used as received. Anhydrous 1,2,4-trichlorobenzene (TCB) was purchased from J&K Scientific and used as received.

2. Synthesis

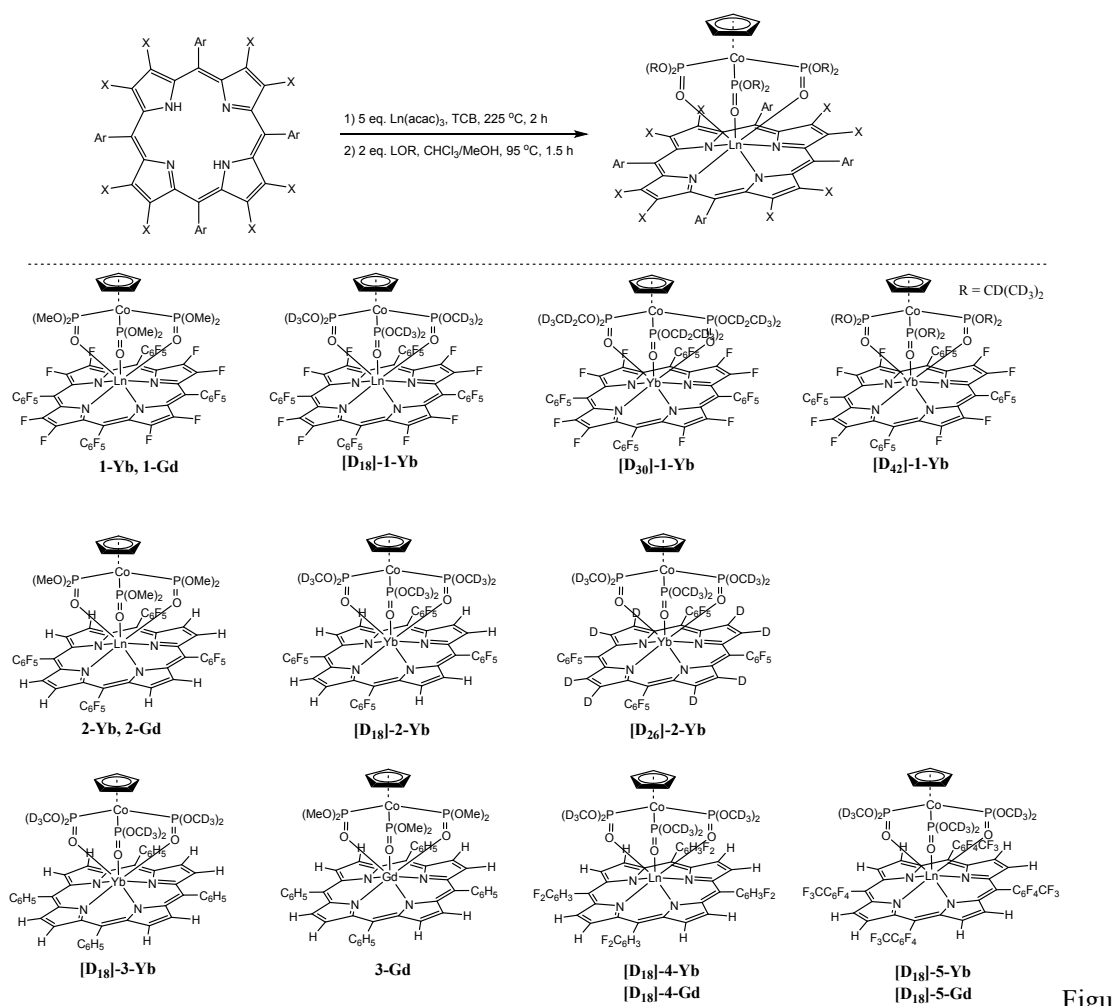
2.1 Porphyrins and Kläui's ligand

β -octafluorinated porphyrins¹ 2,3,7,8,12,13,17,18-Octafluoro-5,10,15,20-tetrakis(pentafluorophenyl)porphyrin (F28TPP), 2,3,7,8,12,13,17,18-Octafluoro-5,10,15,20-tetrakis(phenyl)porphyrin (F8TPP), 2,3,7,8,12,13,17,18-Octafluoro-5,10,15,20-tetrakis(*p*-chlorophenyl)porphyrin, 2,3,7,8,12,13,17,18-Octafluoro-5,10,15,20-tetrakis(4-trifluoromethylphenyl)porphyrin, 2,3,7,8,12,13,17,18-Octafluoro-5,10,15,20-tetrakis(2,6-difluorophenyl)porphyrin and deuterated Kläui's ligand² (D atom > 99%) were synthesized according to literature methods.

2.2 Porphyrinate lanthanide complexes

Porphyrinate lanthanide complexes were prepared via literature reports.³ Porphyrin (0.03 mmol) and Ln(acac)₃·nH₂O (0.15 mmol) in 8 mL 1,2,4-trichlorobenzene (TCB) were refluxed for 2 h under N₂. During the reaction process, the luminescence of porphyrin free base gradually vanished. After cooling to room temperature, the reaction mixture was eluted with petroleum ether, CH₂Cl₂, CH₂Cl₂/MeOH (5/1) sequentially to give TCB, unreacted porphyrin free base and lanthanide porphyrin complexes in order by flash silica gel chromatography. The lanthanide complex and two equivalent Kläui ligand L_{OR} were reacted at 60 °C in 10 mL CHCl₃/MeOH (1/1) for 1.5 h. Then the product with the general formula (F_nTPP)Ln(LOR) was isolated by silica gel chromatography and

recrystallized from CH₂Cl₂ / n-hexane.



Fig

re S1. Synthesis of porphyrinate lanthanide complexes.

Complex 1-Yb. Yield 85% (over two steps, based on the amount of porphyrin free base). Crystal for X-ray analysis was obtained by slow evaporation hexane into a CHCl₃ solution.

¹H NMR (300 MHz, CDCl₃) δ 6.47 (s, 18H), -5.51 (s, 5H). ¹⁹F NMR (282 MHz, CDCl₃) δ -131.04 (d, *J* = 20.8 Hz, 4F), -136.92 (s, 8F), -139.72 (dd, *J* = 23.7, 5.5 Hz, 4F), -150.33 (t, *J* = 20.7 Hz, 4F), -160.22 (t, *J* = 18.2 Hz, 4F), -161.49 (t, *J* = 19.3 Hz, 4F). ESI-HR-MS: Calcd for C₅₅H₂₄CoF₂₈N₄O₉P₃Yb, [M+H⁺]: 1741.90296. Found: 1741.90253. Anal. Calcd. for C₅₅H₂₃CoF₂₈N₄O₉P₃Yb: C, 37.95; H, 1.33; N, 3.22. Found: C, 38.16; H, 1.42; N, 3.24. IR (KBr, cm⁻¹): 2950, 2361, 1673, 1526, 1500, 1466, 1431, 1335, 1176, 1124, 1108, 1047, 1014, 991, 960, 846, 801, 786, 738, 676, 633, 591. UV/Vis (CH₂Cl₂, 25 °C): λ_{max} (log ε, M⁻¹ cm⁻¹): 414(5.60), 544(4.25).

Complex [D18]-1-Yb. Yield 67% (over two steps, based on the amount of porphyrin free base).

¹H NMR (400 MHz, CDCl₃) δ -5.60 (s, 5H). ¹⁹F NMR (377 MHz, CDCl₃) δ -130.52 (dd, *J* = 23.4, 7.7 Hz, 4F), -136.32 (s, 8F), -139.21 (dd, *J* = 24.0, 7.6 Hz, 4F), -149.80 (t, *J* = 20.4 Hz, 4F), -159.68 (t, *J* = 18.4 Hz, 4F), -160.97 (t, *J* = 20.2 Hz, 4F). ESI-HR-MS: Calcd for C₅₅H₆D₁₈CoF₂₈N₄O₉P₃Yb, [M+H⁺]: 1760.01594. Found: 1760.01884. IR (KBr, cm⁻¹): 3056, 2243, 2074, 1659, 1600, 1463, 1444, 1360,

1329, 1172, 1146, 1115, 1071, 1042, 1023, 1007, 920, 846, 779, 747, 700, 663, 608, 576. UV/Vis (CH₂Cl₂, 25 °C): λ_{\max} (log ϵ , M⁻¹ cm⁻¹): 414(5.51), 544(4.23).

Complex **[D₃₀]-1-Yb**. Yield 70% (over two steps, based on the amount of porphyrin free base).

¹H NMR (400 MHz, CDCl₃) δ -5.72 (s, 5H). ¹⁹F NMR (377 MHz, CDCl₃) δ -131.13 (d, J = 18.5 Hz, 4F), -137.09 (s, 8F), -139.42 (dd, J = 24.2, 7.5 Hz, 4F), -149.92 (t, J = 20.4 Hz, 4F), -160.21 (t, J = 18.7 Hz, 4F), -161.00 (t, J = 19.4 Hz, 4F). ESI-HR-MS: Calcd for C₆₁H₆D₃₀CoF₂₈N₄O₉P₃Yb, [M+H⁺]: 1856.18516. Found: 1856.18881. IR (KBr, cm⁻¹): 2295, 2854, 2231, 1671, 1526, 1499, 1467, 1430, 1362, 1335, 1262, 1175, 1127, 1111, 1091, 1050, 1010, 991, 959, 929, 842, 801, 729, 696, 676, 619, 578, 492, 420. UV/Vis (CH₂Cl₂, 25 °C): λ_{\max} (log ϵ , M⁻¹ cm⁻¹): 416(5.39), 546(4.13).

Complex **[D₄₂]-1-Yb**. Yield 40% (over two steps, based on the amount of porphyrin free base). The poor solubility of the compound prevents molar extinction coefficient determination. ¹H NMR (400 MHz, CDCl₃) δ -6.12 (s, 5H). ¹⁹F NMR (377 MHz, CDCl₃) δ -129.52 (m, 4F), -137.49 (s, 8F), -140.30 – -140.67 (m, 4F), -150.04 (t, J = 20.4 Hz, 4F), -160.28 (m, 4F), -160.95 – -161.42 (m, 4F). ESI-HR-MS: Calcd for C₇₇H₆D₄₂CoF₂₈N₄O₉P₃Yb, [M+H⁺]: 1952.35438. Found: 1952.35762. IR (KBr, cm⁻¹): 2233, 1675, 1640, 1527, 1499, 1466, 1430, 1334, 1262, 1230, 1175, 1119, 1105, 1069, 1047, 992, 975, 960, 935, 916, 836, 801, 750, 676, 635, 608, 577, 526, 473. UV/Vis (CH₂Cl₂, 25 °C): λ_{\max} (log ϵ , M⁻¹ cm⁻¹): 420, 551.

Complex **1-Gd**. Yield 57% (over two steps, based on the amount of porphyrin free base). Crystal for X-ray analysis was obtained by slow evaporation hexane into a CHCl₃ solution.

ESI-HR-MS: Calcd for C₅₅H₂₄CoF₂₈N₄O₉P₃Gd, [M+H⁺]: 1725.88820. Found: 1725.89035. Anal. Calcd. for C₅₅H₂₃CoF₂₈N₄O₉P₃Gd: C, 38.30; H, 1.34; N, 3.25. Found: C, 38.71; H, 1.54; N, 3.25. IR (KBr, cm⁻¹): 2950, 1668, 1525, 1501, 1459, 1430, 1333, 1175, 1140, 1121, 1106, 1047, 1013, 991, 958, 847, 801, 785, 736, 675, 632, 590. UV/Vis (CH₂Cl₂, 25 °C): λ_{\max} (log ϵ , M⁻¹ cm⁻¹): 414(5.45), 544(4.22).

Complex **2-Yb**. Yield 74% (over two steps, based on the amount of porphyrin free base).

¹H NMR (400 MHz, CDCl₃) δ 14.96 (s, 8H), 6.34 (s, 18H), -4.98 (s, 5H). ¹⁹F NMR (377 MHz, CDCl₃) δ -128.39 (d, J = 20.8 Hz, 4F), -136.42 (dd, J = 24.9, 8.0 Hz, 4F), -151.61 (t, J = 20.4 Hz, 4F), -159.42 – -160.44 (m, 4F), -161.43 (t, J = 20.6 Hz, 4F). ESI-HR-MS: calcd for C₅₅H₃₂CoF₂₀N₄O₉P₃Yb, [M+H⁺]: 1597.97834; Found: 1597.97870. Anal. Calcd. for C₅₅H₃₁CoF₂₀YbN₄O₉P₃+CH₃OH: C, 41.29; H, 2.17; N, 3.44; found: C, 42.43; H, 2.39; N, 3.44. IR (KBr, cm⁻¹): 2947, 2841, 1727, 1650, 1528, 1519, 1487, 1442, 1377, 1331, 1286, 1158, 1131, 1075, 1047, 1012, 988, 935, 836, 801, 759, 733, 710, 620, 588, 529, 412. UV/Vis (CH₂Cl₂, 25 °C): λ_{\max} (log ϵ , M⁻¹ cm⁻¹): 422(5.77), 553(4.44).

Complex **[D₁₈]-2-Yb**. Yield 72% (over two steps, based on the amount of porphyrin free base).

¹H NMR (400 MHz, CDCl₃) δ 14.96 (s, 8H), -4.99 (s, 5H). ¹⁹F NMR (377 MHz, CDCl₃) δ -128.44 (d, J = 18.2 Hz, 4F), -136.41 (dd, J = 24.7, 8.0 Hz, 4F), -151.61 (t, J = 20.5 Hz, 4F), -159.75 – -160.46 (m, 4F), -161.18 – -161.84 (m, 4F). ESI-HR-MS: calcd for C₅₅H₁₄D₁₈CoF₂₀N₄O₉P₃Yb, [M+H⁺]: 1616.09132; Found: 1616.09175. IR (KBr, cm⁻¹): 2923, 2852, 2246, 2076, 1728, 1651, 1530, 1520,

1486, 1443, 1377, 1331, 1267, 1137, 1120, 1074, 1047, 1025, 987, 956, 843, 835, 801, 760, 745, 703, 581. UV/Vis (CH₂Cl₂, 25 °C): λ_{\max} (log ϵ , M⁻¹ cm⁻¹): 422(5.77), 553(4.44).

Complex [D₂₆]-2-Yb. Yield 70% (over two steps, based on the amount of porphyrin free base). The isotopic purity of 2,3,7,8,12,13,17,18-octadeuterium-5,10,15,20-tetrakis(pentafluorophenyl)porphyrin was estimated to be > 90% based on ¹H NMR spectroscopy analysis.

¹H NMR (400 MHz, CDCl₃) δ -4.90 (s, 5H). ¹⁹F NMR (377 MHz, Chloroform-*d*) δ -128.51 (d, *J* = 24.3 Hz, 4F), -136.40 (d, *J* = 23.6 Hz, 4F), -151.64 (t, *J* = 20.4 Hz, 4F), -160.18 (t, *J* = 18.7 Hz, 4F), -161.44 (t, *J* = 22.0 Hz, 4F). ESI-HR-MS: calcd for C₅₅H₆D₂₆CoF₂₀N₄O₉P₃Yb, [M+H⁺]: 1624.14153; Found: 1624.13842. IR (KBr, cm⁻¹): 2361, 2077, 1649, 1523, 1520, 1496, 1433, 1330, 1143, 1075, 1041, 1025, 988, 944, 866, 839, 747, 703, 581. UV/Vis (CH₂Cl₂, 25 °C): λ_{\max} (log ϵ , M⁻¹ cm⁻¹): 422(5.57), 553(4.28), 588 (3.52).

Complex 2-Gd. Yield 50% (over two steps, based on the amount of porphyrin free base). ESI-HR-MS: calcd for C₅₅H₃₂CoF₂₀GdN₄O₉P₃, [M+H⁺]: 1581.96358. Found: 1581.96435; Anal. Calcd. for C₅₅H₃₁CoF₂₀GdN₄O₉P₃+CH₃OH: C, 41.70; H, 2.19; N, 3.47. Found: C, 42.55; H, 2.31; N, 3.54. IR (KBr, cm⁻¹): 2946, 1650, 1525, 1498, 1330, 1125, 1075, 1047, 1013, 988, 935, 836, 800, 759, 731, 588. UV/Vis (CH₂Cl₂, 25 °C): λ_{\max} (log ϵ , M⁻¹ cm⁻¹): 422(5.80), 553(4.45).

Complex [D₁₈]-3-Yb. Yield 50% (over two steps, based on the amount of porphyrin free base). Crystal for X-ray analysis was obtained by slow evaporation of a CH₂Cl₂/MeOH (1/1) solution.

¹H NMR (300 MHz, CDCl₃) δ 16.99 (s, 4H), 10.66 (s, 4H), 9.56 (s, 4H), 8.99 (s, 8H), -5.22 (s, 5H). ¹⁹F NMR (282 MHz, Chloroform-*d*) δ -132.93 (s, 8F). ESI-HR-MS: Calcd for C₅₅H₂₆D₁₈CoF₈N₄O₉P₃Yb, [M+H⁺]: 1400.20438. Found: 1400.20522. IR (KBr, cm⁻¹): 2926, 2856, 2248, 2079, 1673, 1526, 1500, 1467, 1431, 1362, 1335, 1176, 1133, 1113, 1068, 1048, 1026, 991, 960, 921, 845, 801, 750, 730, 708, 676, 633, 609, 582, 528. UV/Vis (CH₂Cl₂, 25 °C): λ_{\max} (log ϵ , M⁻¹ cm⁻¹): 416(5.58), 546(4.20), 587 (3.89).

Complex 3-Gd. Yield 20% (over two steps, based on the amount of porphyrin free base). Crystal for X-ray analysis was obtained by slow evaporation of a CH₂Cl₂/MeOH (1/1) solution.

ESI-HR-MS: Calcd for C₅₅H₄₃CoF₈GdN₄O₉P₃, [M+H⁺]: 1366.07664. Found: 1366.07605. Anal. Calcd. for C₅₅H₄₃CoF₈GdN₄O₉P₃: C, 48.39; H, 3.18; N, 4.10. Found: C, 48.20; H, 3.29; N, 3.83. IR (KBr, cm⁻¹): 2944, 2360, 2342, 1654, 1601, 1459, 1444, 1356, 1327, 1172, 1147, 1131, 1111, 1038, 1006, 847, 778, 731, 701, 682, 661, 586. UV/Vis (CH₂Cl₂, 25 °C): λ_{\max} (log ϵ , M⁻¹ cm⁻¹): 417(5.54), 547(4.13), 588(3.85)

Complex [D₁₈]-4-Yb. Yield 93% (over two steps, based on the amount of porphyrin free base).

¹H NMR (400 MHz, CDCl₃) δ 10.51 (t, *J* = 7.6 Hz, 4H), 9.45 (s, 4H), 8.15 (t, *J* = 7.9 Hz, 4H), -5.42 (s, 5H). ¹⁹F NMR (377 MHz, CDCl₃) δ -101.65 (s, 4F), -110.73 (s, 4F), -137.61 (s, 8F). ESI-HR-MS: calcd for C₅₅H₁₈D₁₈CoF₁₆N₄O₁₁P₃Yb, [M+H⁺]: 1544.12900; Found: 1544.12715. IR (KBr, cm⁻¹): 2078, 1669, 1626, 1591, 1465, 1360, 1328, 1276, 1237, 1172, 1145, 1116, 1069, 1027, 1003, 922, 845, 792, 748, 705, 663, 606, 580, 510. UV/Vis (CH₂Cl₂, 25 °C): λ_{\max} (log ϵ , M⁻¹ cm⁻¹):

415(5.50), 546(4.25).

Complex **[D₁₈]-4-Gd**. Yield 97% (over two steps, based on the amount of porphyrin free base).

ESI-HR-MS: calcd for C₅₅H₁₈D₁₈CoF₁₆N₄O₁₁P₃Gd, [M+H⁺]: 1528.11425; Found: 1528.11541. IR (KBr, cm⁻¹): 2292, 2077, 1665, 1625, 1591, 1505, 1465, 1385, 1354, 1324, 1276, 1237, 1171, 1144, 1115, 1065, 1045, 1025, 1002, 921, 846, 792, 746, 704, 660, 605, 579, 510, 477. UV/Vis (CH₂Cl₂, 25 °C): λ_{max} (log ε, M⁻¹ cm⁻¹): 415(5.53), 545 (4.22).

Complex **[D₁₈]-5-Yb** Yield 85% (over two steps, based on the amount of porphyrin free base)

¹H NMR (400 MHz, CDCl₃) δ 17.32 (s, 4H), 10.99 (s, 4H), 9.07 (s, 4H), 8.75 (s, 4H), -5.19 (s, 5H).

¹⁹F NMR (377 MHz, CDCl₃) δ -60.84 (s, 12F), -131.44 (s, 8F). ESI-HR-MS: calcd for C₅₉H₂₂D₁₈CoF₂₀N₄O₉P₃Yb, [M+H⁺]: 1672.15392; Found: 1672.15009. IR (KBr, cm⁻¹): 2076, 1665, 1616, 1463, 1408, 1324, 1173, 1147, 1069, 1046, 1022, 843, 747, 704, 665, 580. UV/Vis (CH₂Cl₂, 25 °C): λ_{max} (log ε, M⁻¹ cm⁻¹): 415(5.47), 544 (4.20), 585 (3.64).

Complex **[D₁₈]-5-Gd** Yield 82% (over two steps, based on the amount of porphyrin free base)

ESI-HR-MS: calcd for C₅₉H₂₂D₁₈CoF₂₀N₄O₉P₃Gd, [M+H⁺]: 1656.13916; Found: 1656.13545. IR (KBr, cm⁻¹): 2926, 2075, 1660, 1616, 1459, 1408, 1324, 1172, 1136, 1113, 1069, 1045, 1022, 1001, 844, 746, 703, 664, 579. UV/Vis (CH₂Cl₂, 25 °C): λ_{max} (log ε, M⁻¹ cm⁻¹): 415(5.49), 545 (4.22), 585 (3.72).

2.3 Summary of Crystallographic Data

Table S1. Crystal data and structure refinement

Complex	1-Yb	2-Yb	[D₁₈]-3-Yb
molecular formula	C ₅₅ H ₂₃ CoF ₂₈ N ₄ O ₉ P ₃ Yb	C ₅₅ H ₃₁ CoF ₂₀ N ₄ O ₉ P ₃ Yb	C ₅₅ H ₂₅ D ₁₈ CoF ₈ N ₄ O ₉ P ₃ Yb
formula wt. (g mol ⁻¹)	1740.65	1596.71	1398.92
temperature (K)	180(2)	276.8(1)	180(2)
radiation (λ, Å)	0.71073	0.71073	0.71073
crystal system	monoclinic	orthorhombic	triclinic
space group	<i>C2/c</i>	<i>Cmcm</i>	<i>P</i> $\bar{1}$
<i>a</i> (Å)	24.588(5)	15.8901(4)	12.2948(3)
<i>b</i> (Å)	10.147(2)	19.2041(5)	14.0793(3)
<i>c</i> (Å)	24.582(5)	22.9477(6)	16.6204(4)
α (°)	90	90	72.8693(19)
β (°)	92.11(3)	90	73.873(2)
γ (°)	90	90	77.720(2)
Volume (Å ³)	6129(2)	7002.6(3)	2614.22(11)
<i>Z</i>	4	4	2
ρ_{calcd} (g cm ⁻³)	1.886	1.739	1.777
μ (mm ⁻¹)	2.010	1.935	2.278
F(000)	3388	3596	1374
crystal size (mm ³)	0.20×0.18×0.11	0.21×0.17×0.15	0.25×0.14×0.08
Theta range	2.75, 27.48	3.817, 29.010	2.722, 27.452
reflections collected	50103	14681	39776
independent reflections	7019	3282	11924
Completeness	0.999	0.997	99.85
goodness-of-fit on F ²	1.052	1.111	1.047
final R indices [R > 2σ(I)]	0.0286, 0.0681	0.0501, 0.1492	0.0762, 0.1875
R indices (all data)	0.0335, 0.0719	0.0524, 0.1512	0.0885, 0.1999
largest diff. peak and hole (e Å ⁻³)	1.207, -0.793	2.922, -1.773	12.480, -3.451

Table S2. Selected bond length for ytterbium complexes.

Complex	1-Yb	2-Yb	[D ₁₈]-3-Yb
Yb-O / Å	2.205(4)	2.236(8)	2.220(7)
	2.236(4)	2.236(8)	2.232(6)
	2.224(4)	2.270(11)	2.245(7)
Yb-N / Å	2.380(2)	2.363(6)	2.369(7)
	2.376(2)	2.364(7)	2.359(6)
	2.380(2)	2.368(7)	2.375(6)
	2.376(2)	2.368(7)	2.378(6)
Yb-N4 plane / Å	1.180(1)	1.184(1)	1.169(1)

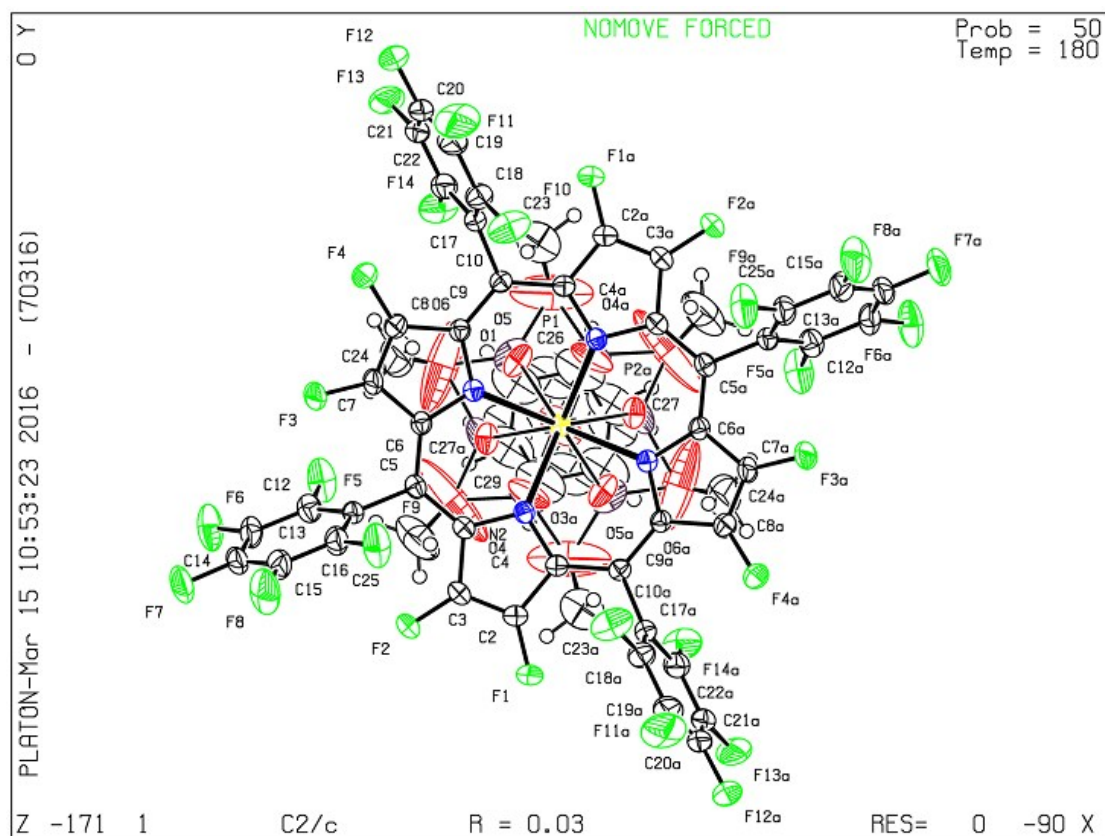


Figure SS2. Perspective drawing of **1-Yb** (CCDC 1501198) with 50% ellipsoids.

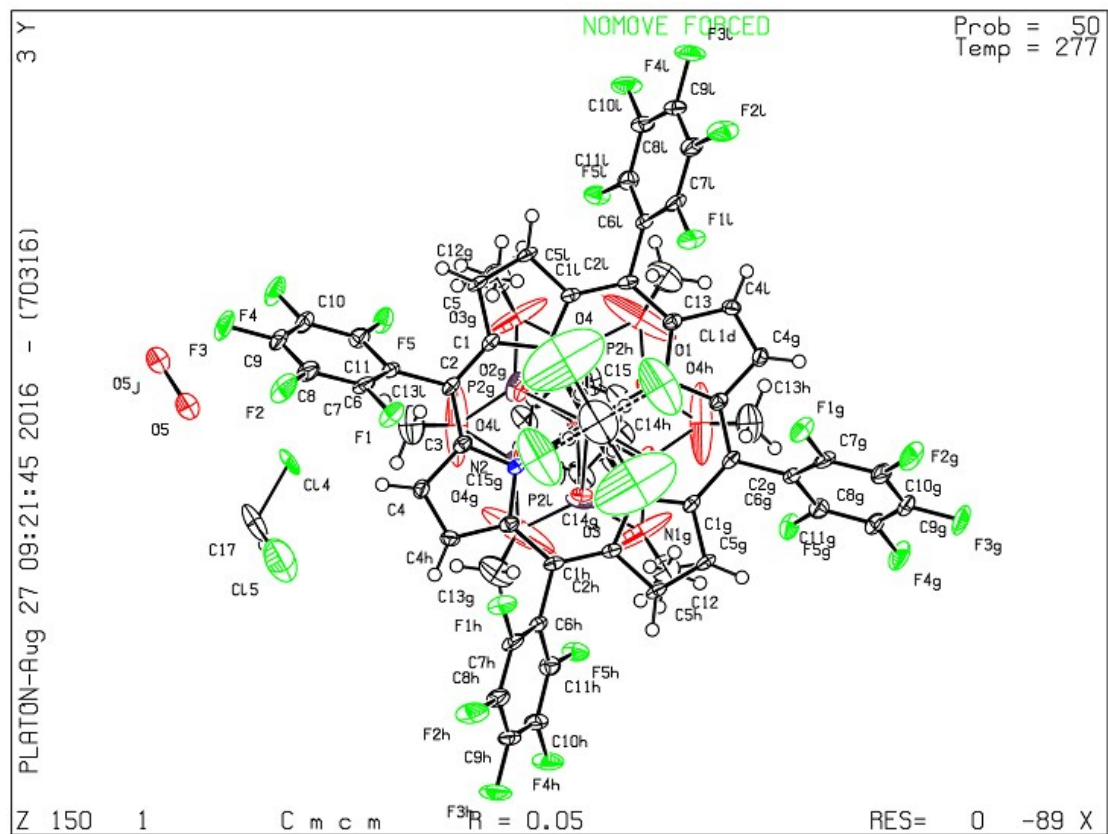


Figure S3. Perspective drawing of **2-Yb** (CCDC 1501199) with 50% ellipsoids.

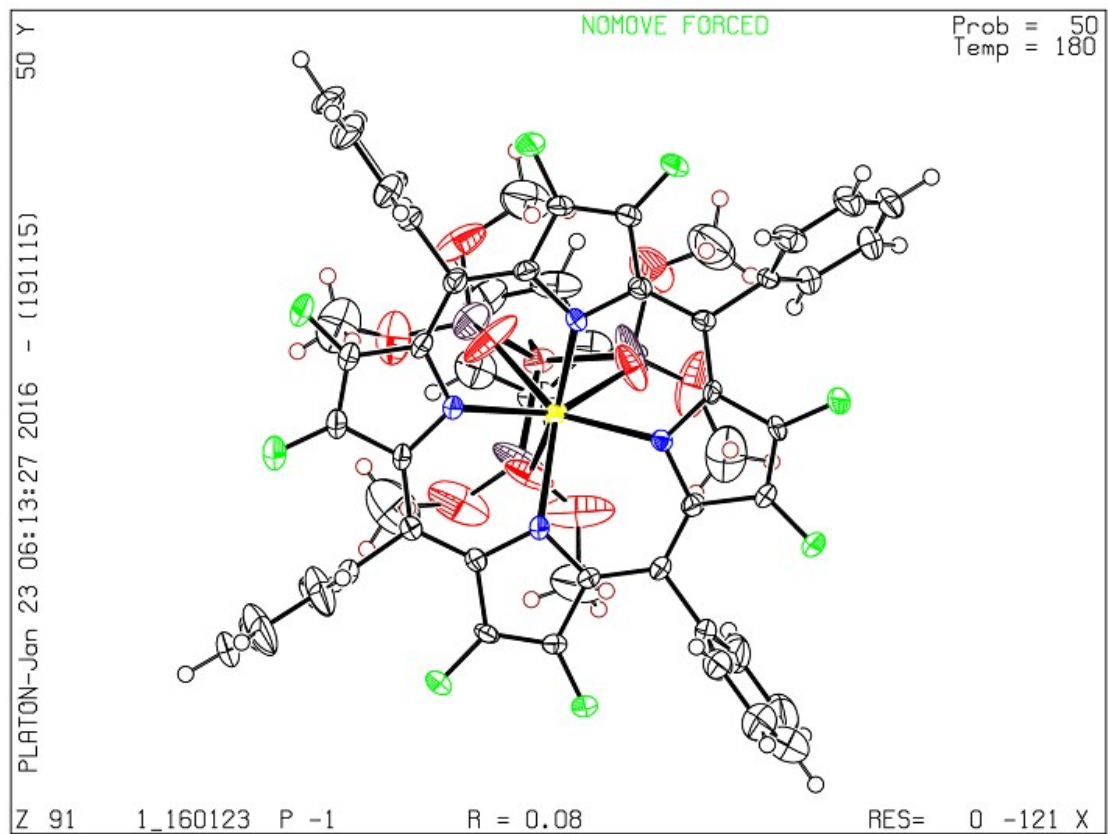


Figure S4. Perspective drawing of $[D_{18}]$ -3-Yb (CCDC 1501200) with 50% ellipsoids.

2.4 NMR spectra

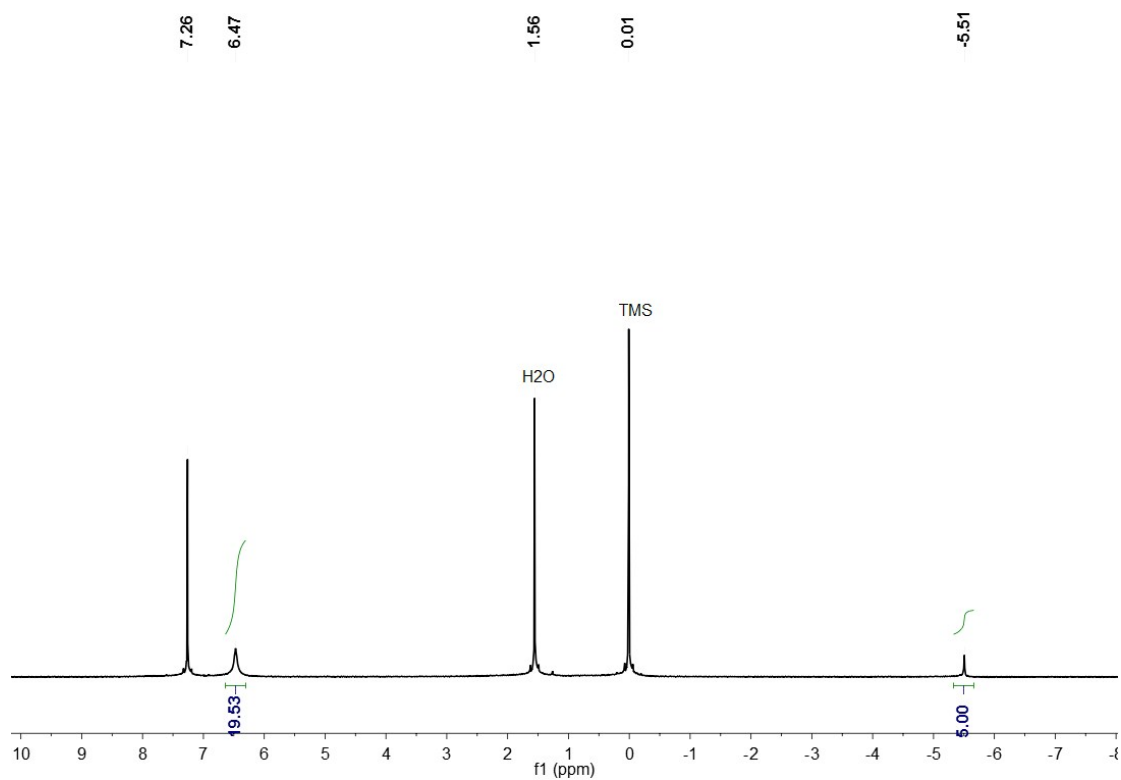


Figure S5. ¹H NMR (CDCl₃) of **1-Yb**

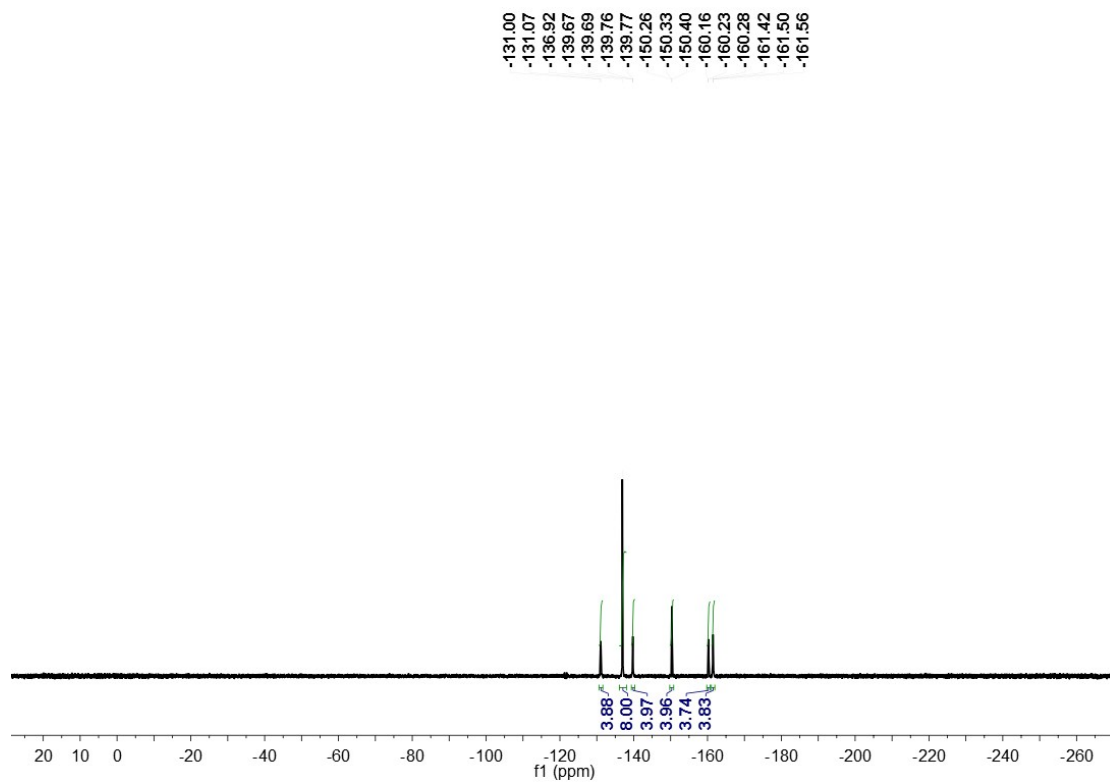


Figure S6. ¹⁹F NMR (CDCl₃) of **1-Yb**

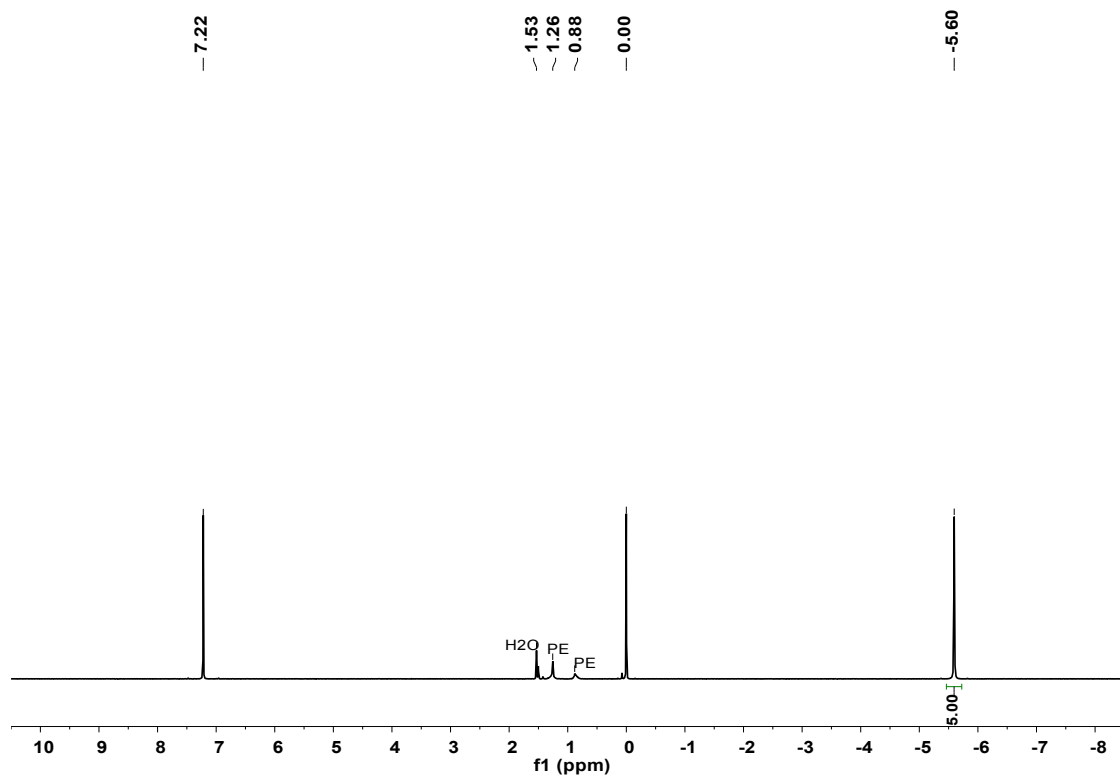


Figure S7. ¹H NMR (CDCl₃) of [D₁₈]-1-Yb

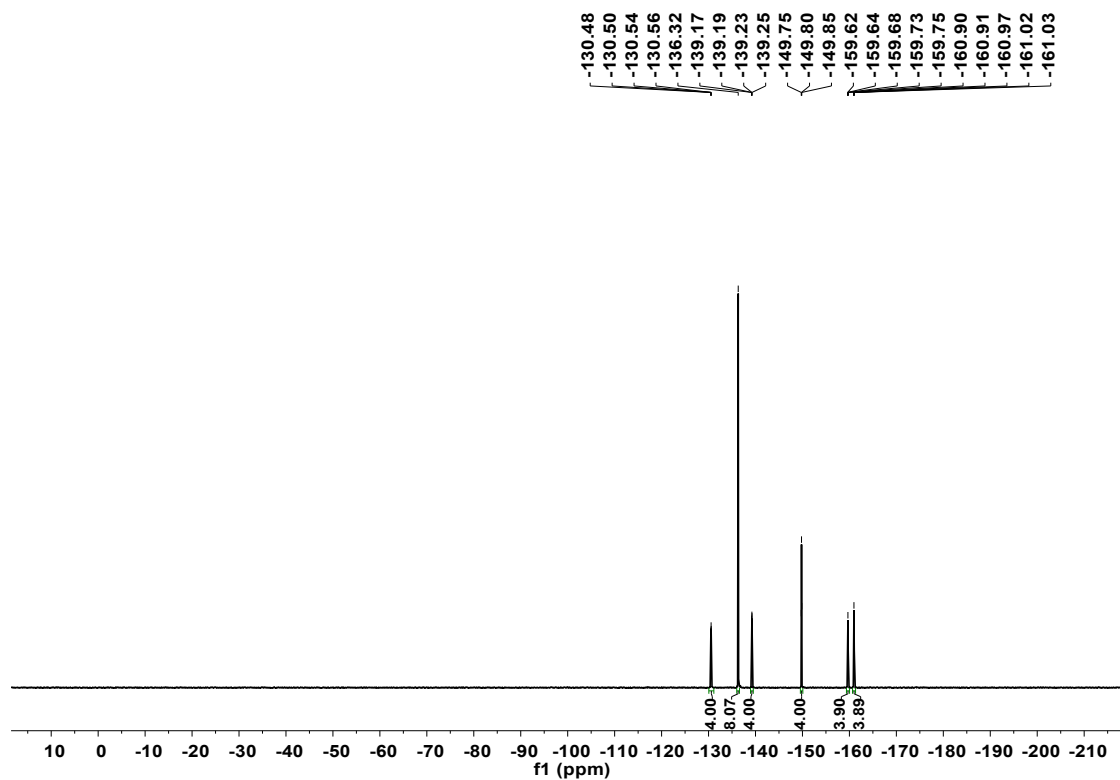


Figure S8. ¹⁹F NMR (CDCl₃) of [D₁₈]-1-Yb

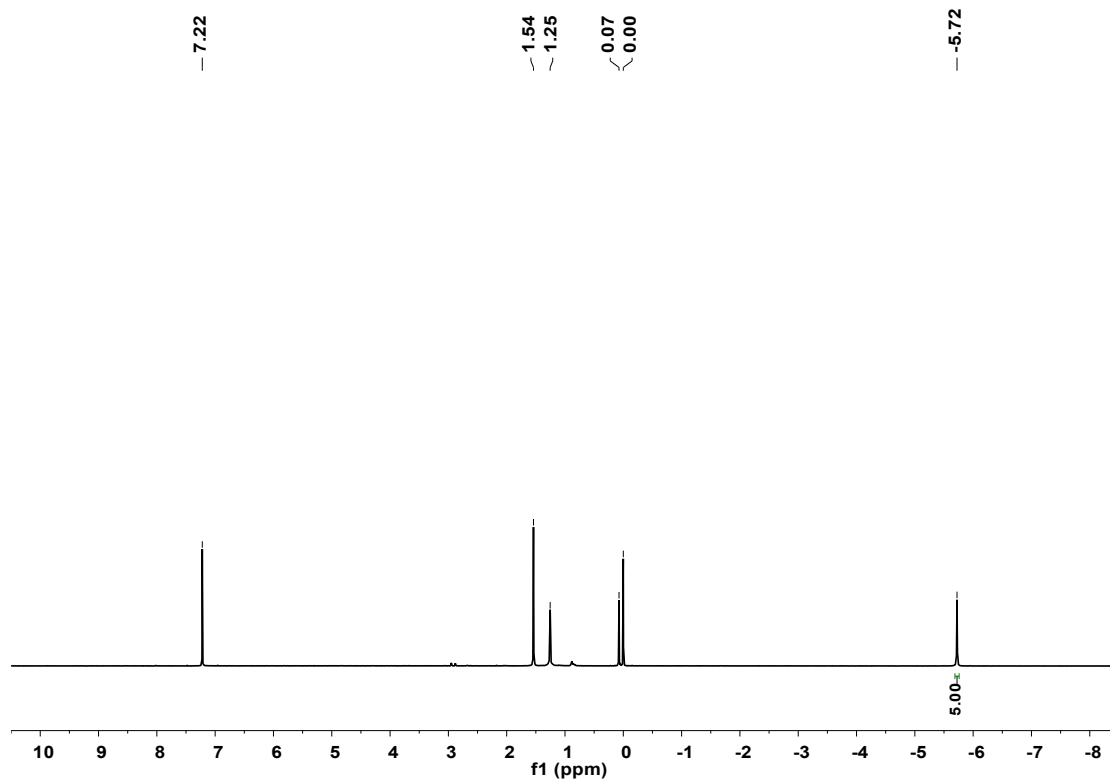


Figure S9. ^1H NMR (CDCl_3) of $[\text{D}_{30}]\text{-1-Yb}$

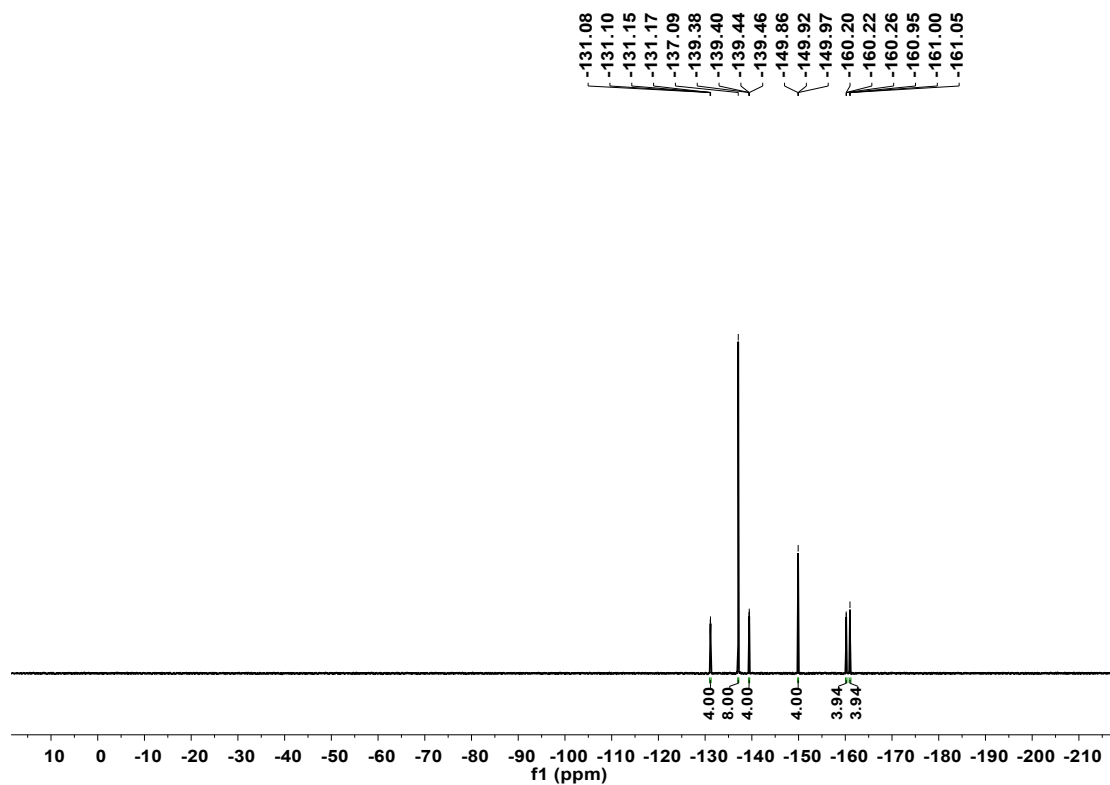


Figure S10. ^{19}F NMR (CDCl_3) of $[\text{D}_{30}]\text{-1-Yb}$

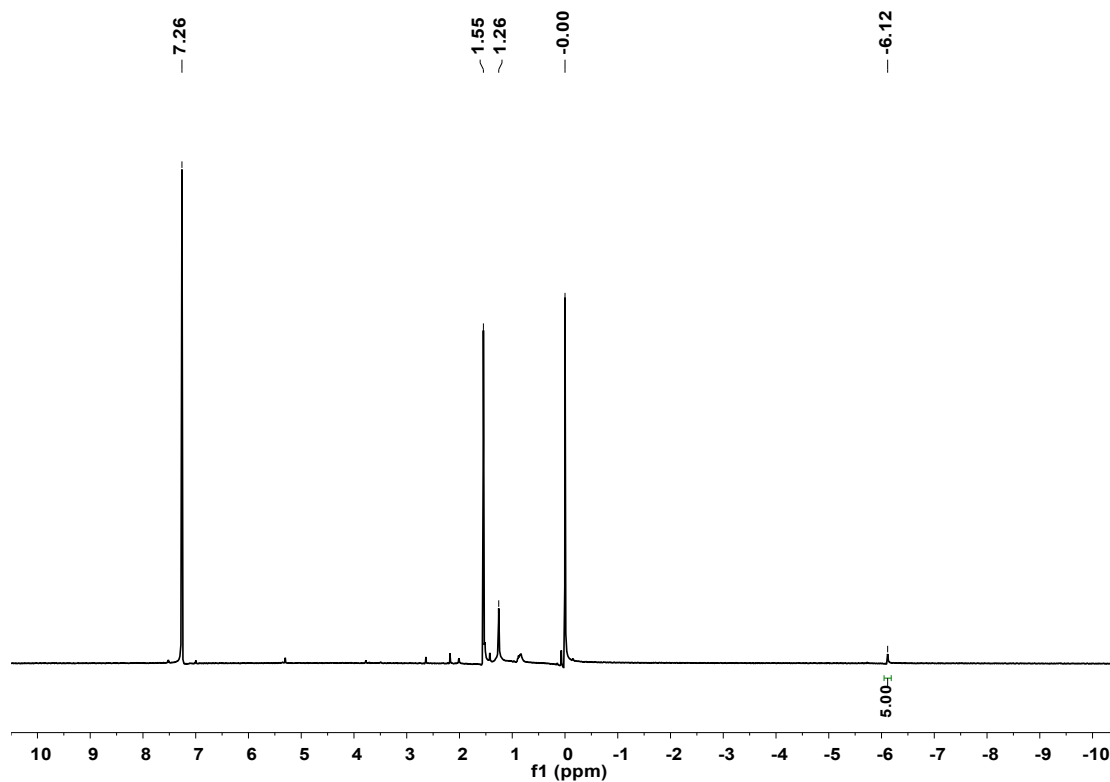


Figure S11. 1H NMR ($CDCl_3$) of $[D_{42}]-1-Yb$

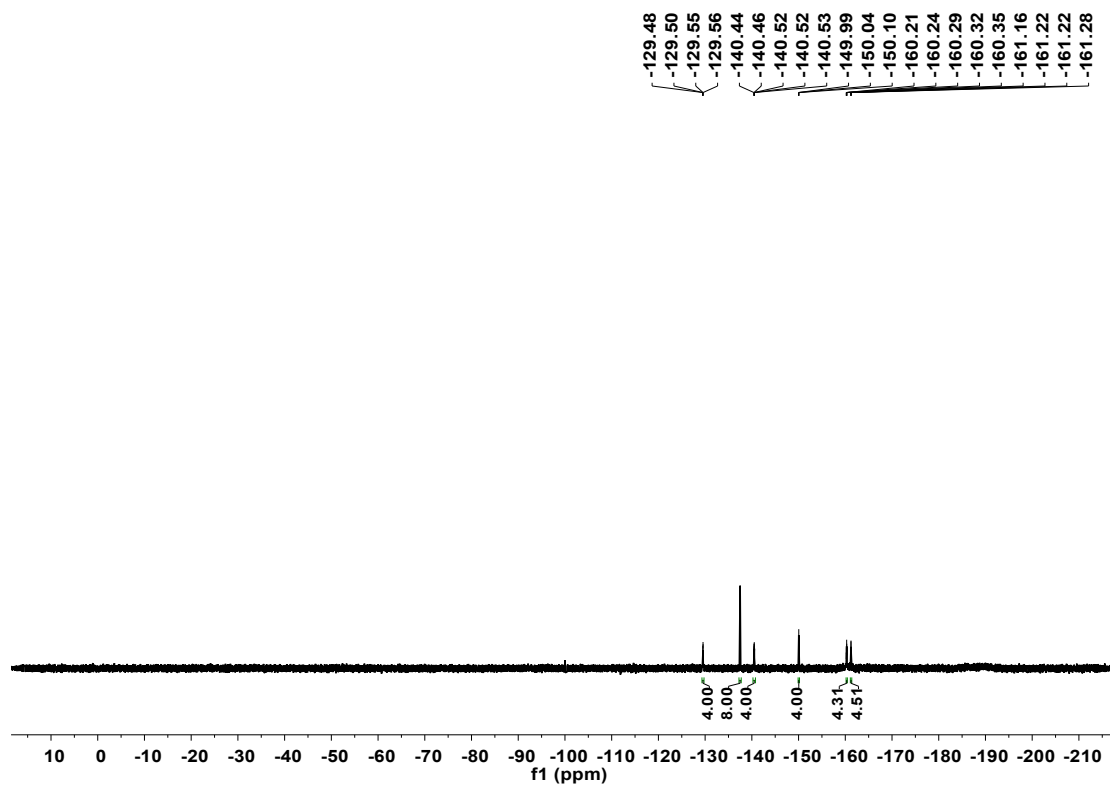


Figure S12. ^{19}F NMR ($CDCl_3$) of $[D_{42}]-1-Yb$

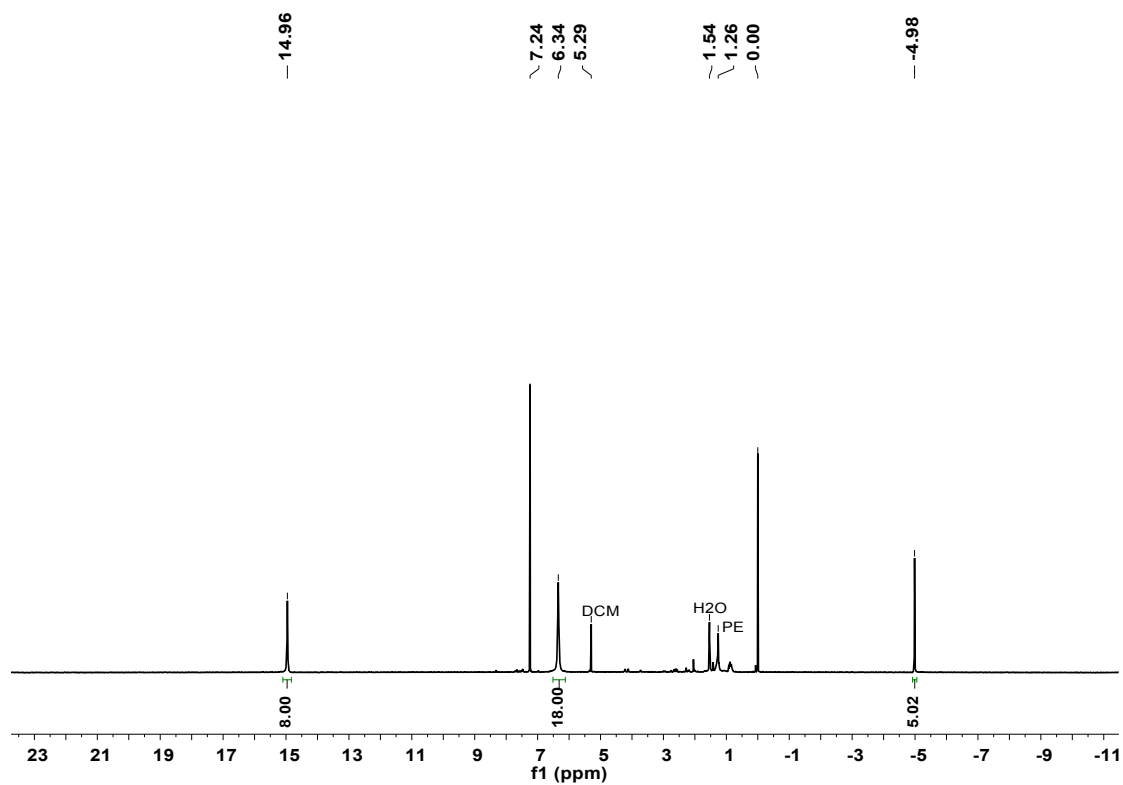


Figure S13. ¹H NMR (CDCl₃) of **2-Yb**

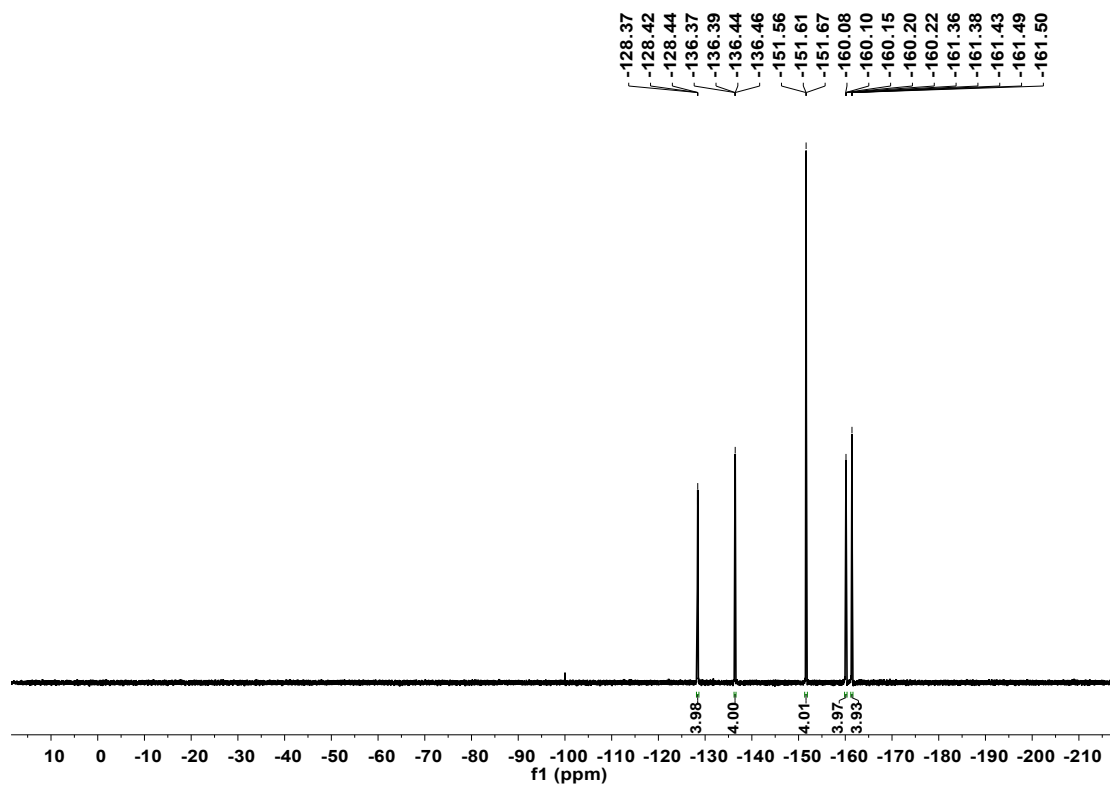


Figure S14. ¹⁹F NMR (CDCl₃) of **2-Yb**

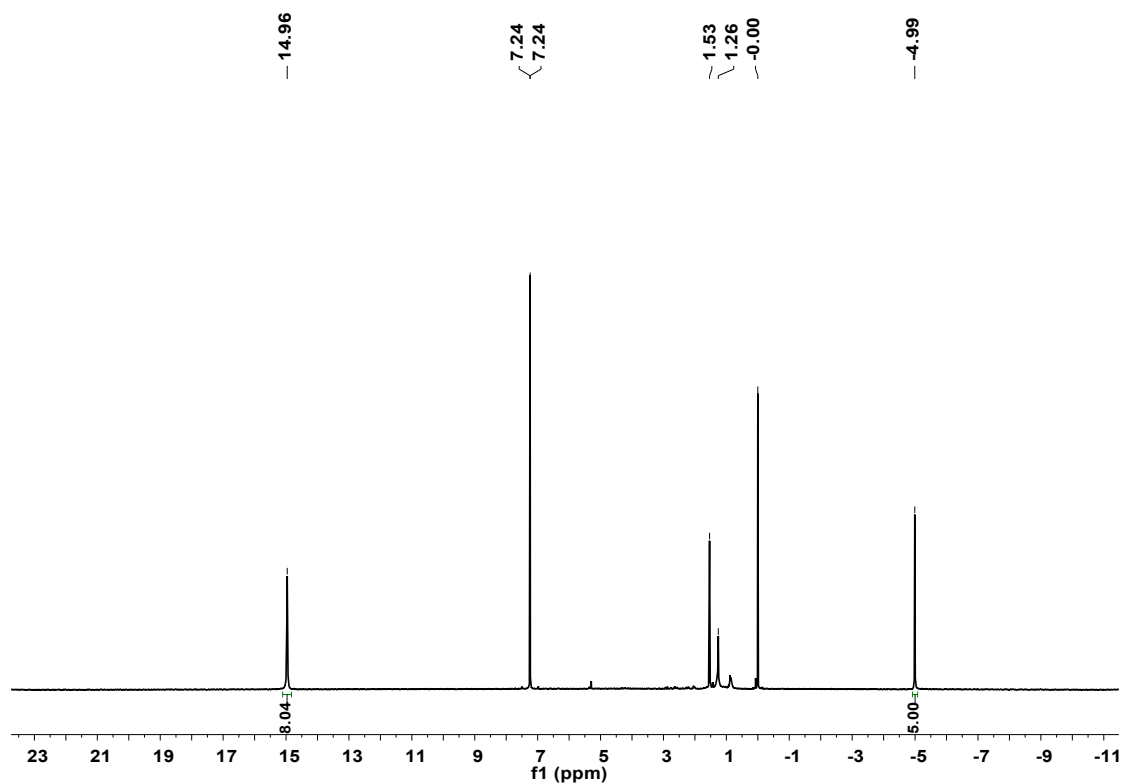


Figure S15. ^1H NMR (CDCl_3) of $[\text{D}_{18}]\text{-2-Yb}$

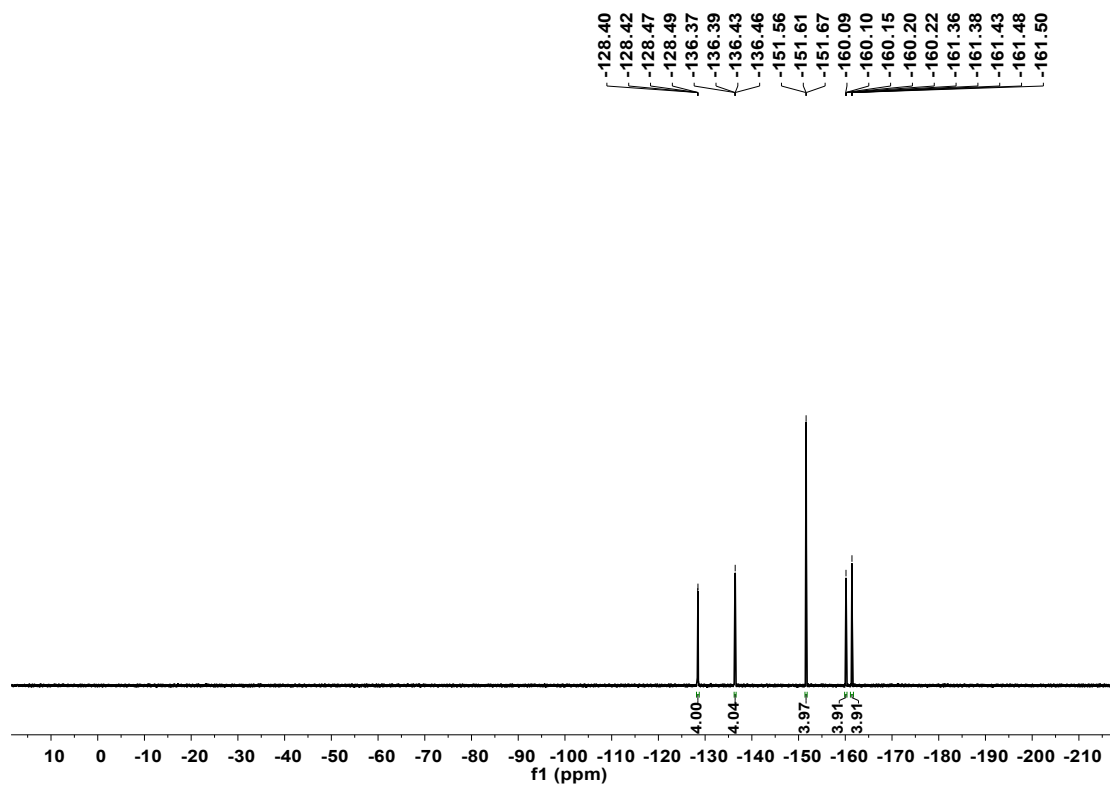


Figure S16. ^{19}F NMR (CDCl_3) of $[\text{D}_{18}]\text{-2-Yb}$

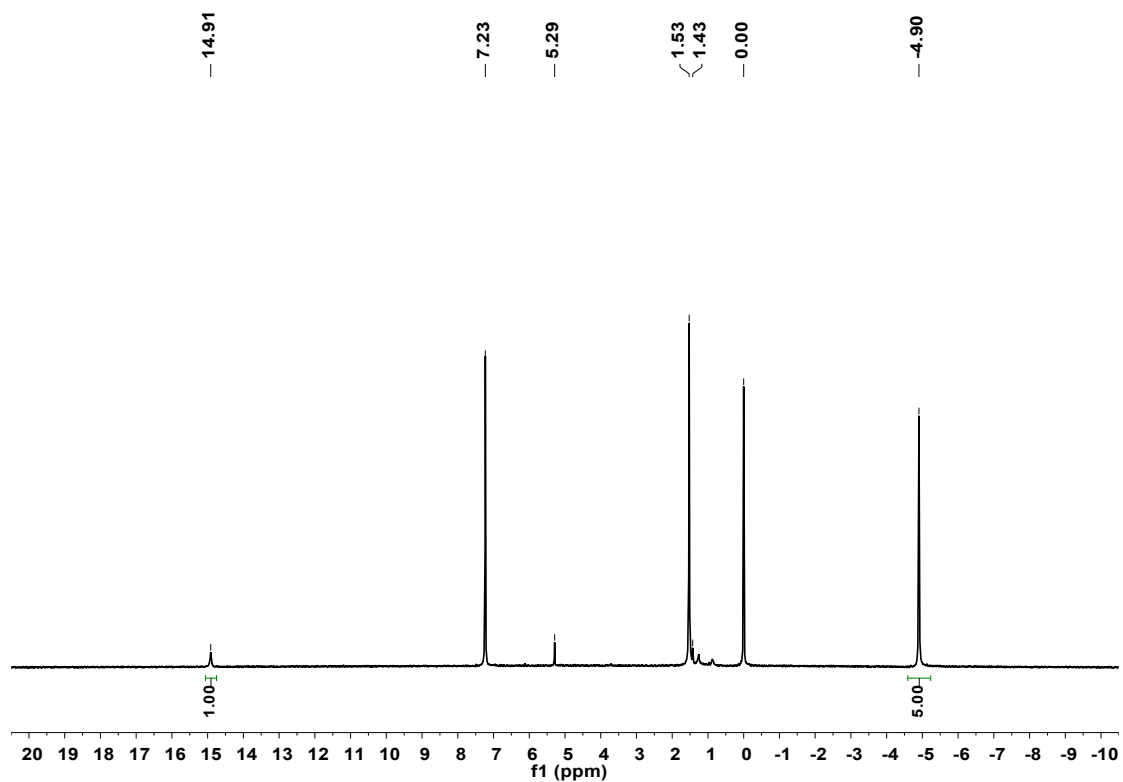


Figure S17. ^1H NMR (CDCl_3) of $[\text{D}_{26}]\text{-2-Yb}$

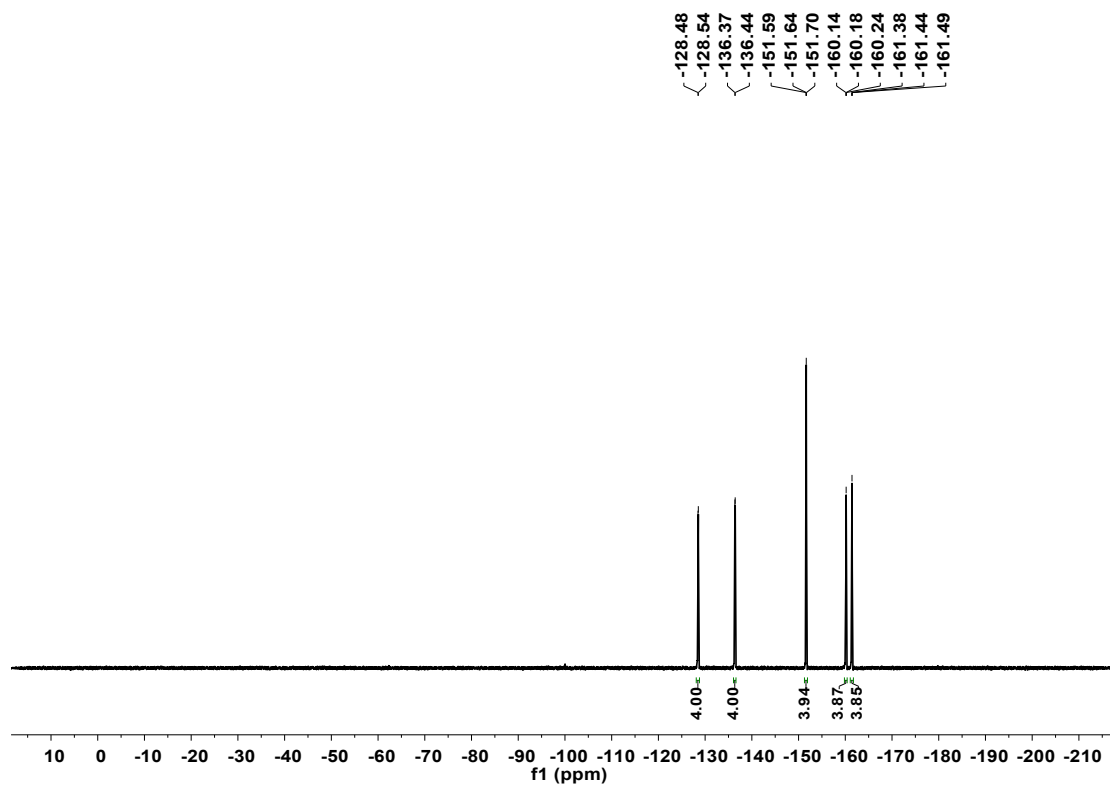


Figure S18. ^{19}F NMR (CDCl_3) of $[\text{D}_{26}]\text{-2-Yb}$

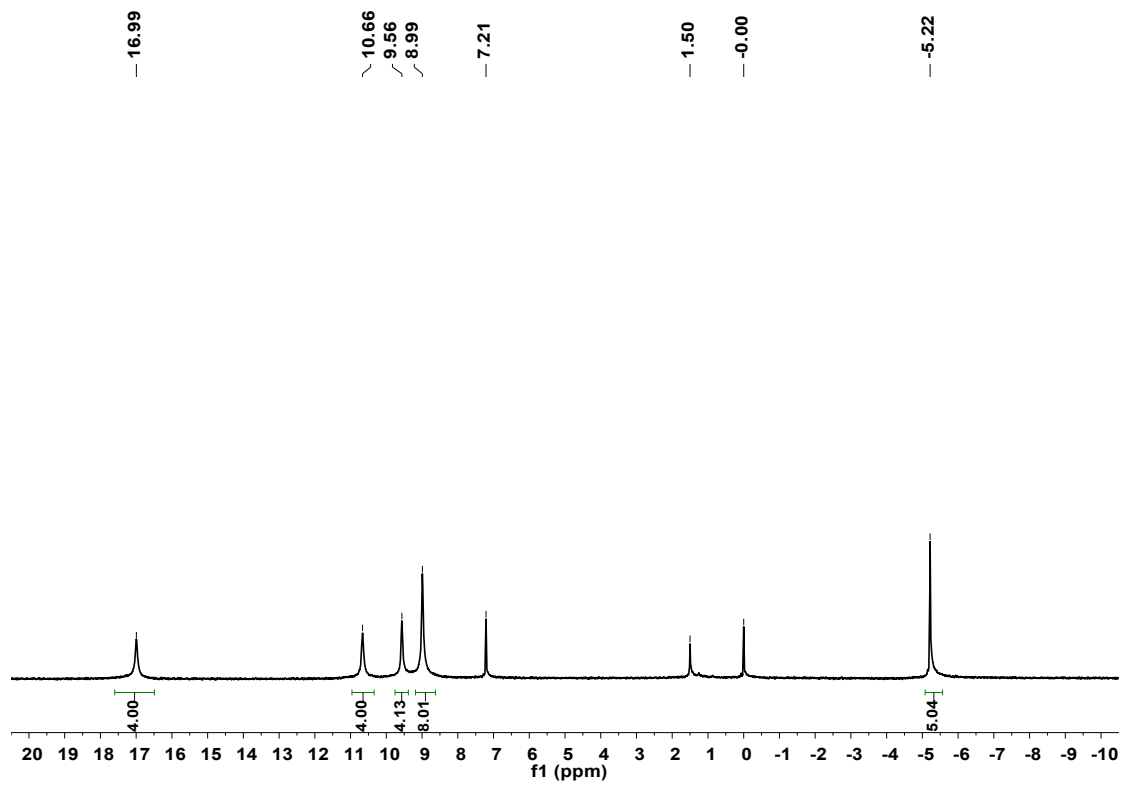


Figure S19. ^1H NMR (CDCl_3) of $[\text{D}_{18}]\text{-3-Yb}$

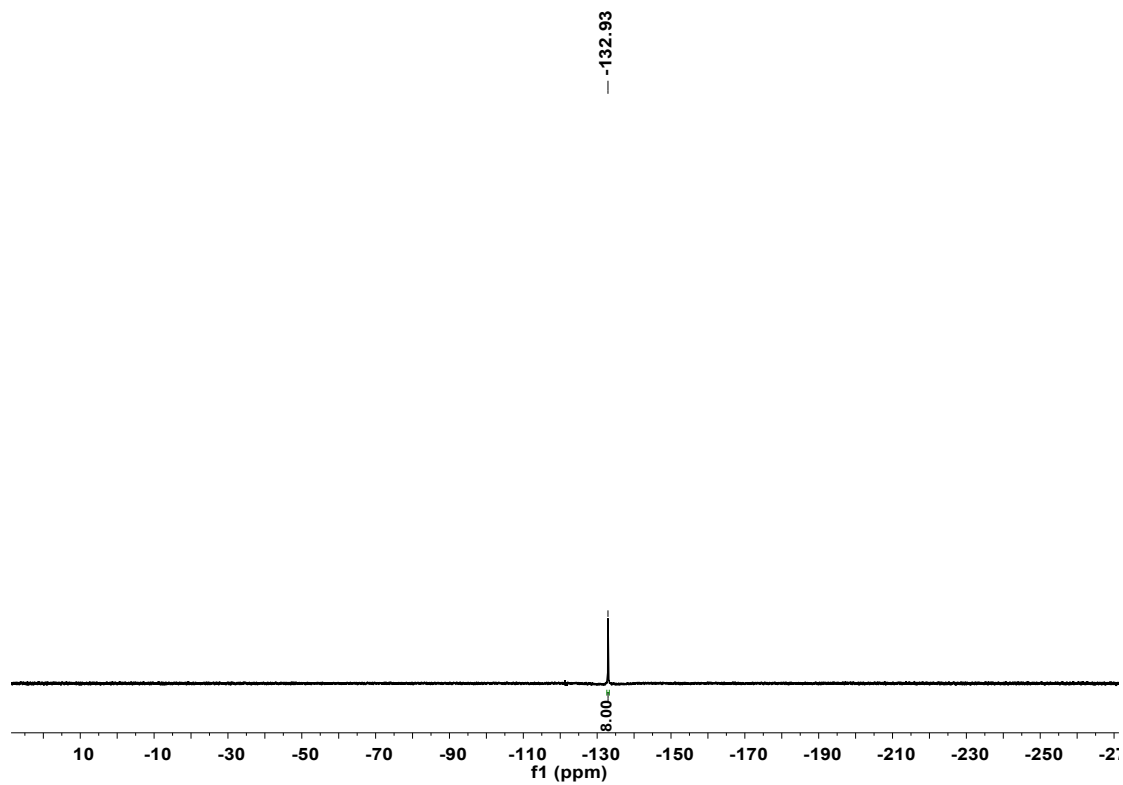


Figure S20. ^{19}F NMR (CDCl_3) of $[\text{D}_{18}]\text{-3-Yb}$

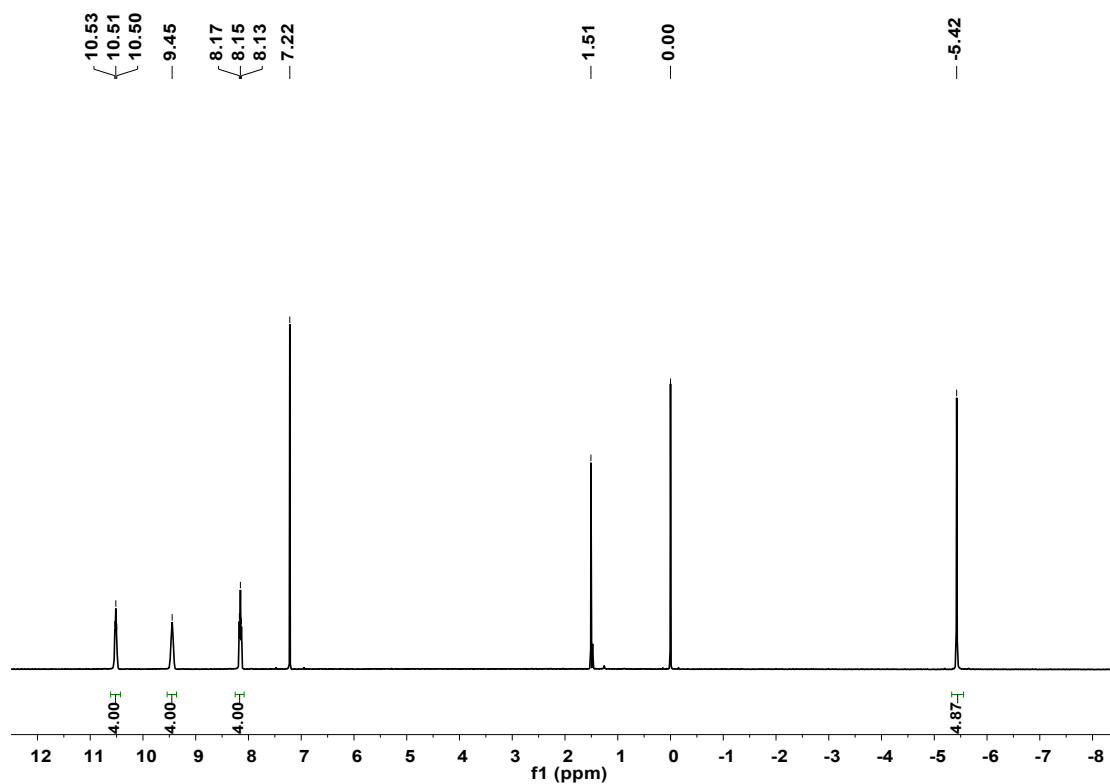


Figure S21. ^1H NMR (CDCl_3) of $[\text{D}_{18}]\text{-4-Yb}$

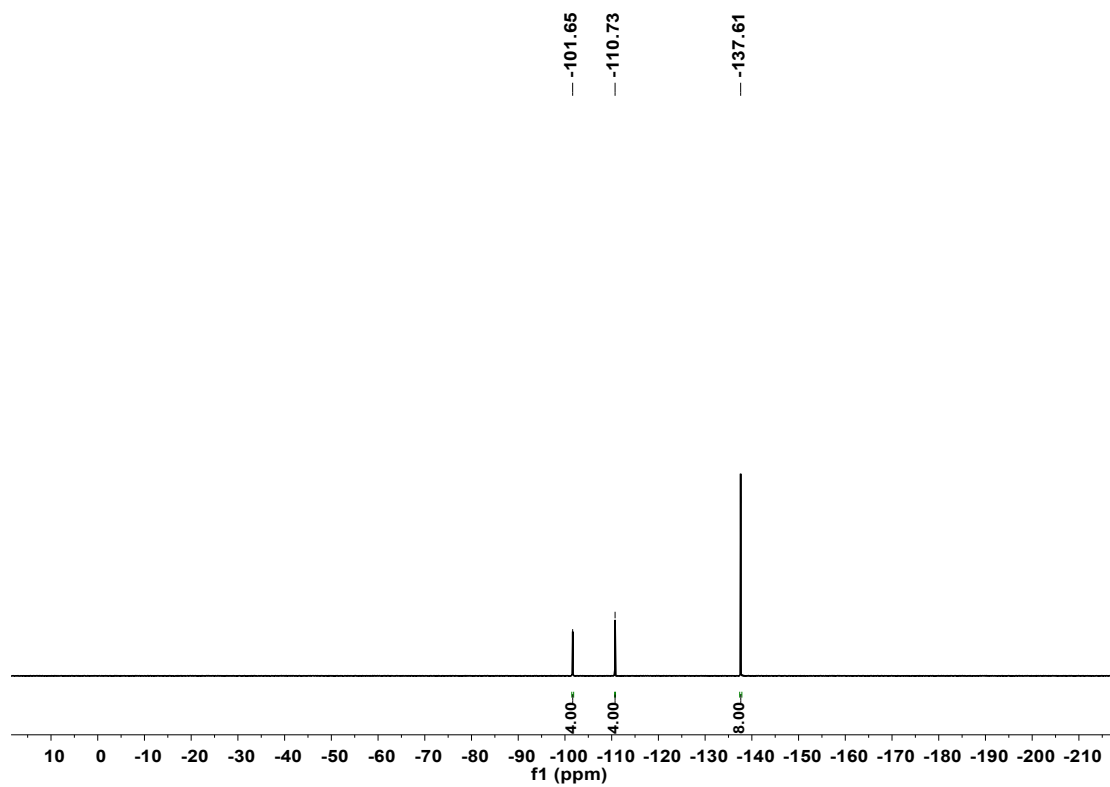


Figure S22. ^{19}F NMR (CDCl_3) of $[\text{D}_{18}]\text{-4-Yb}$

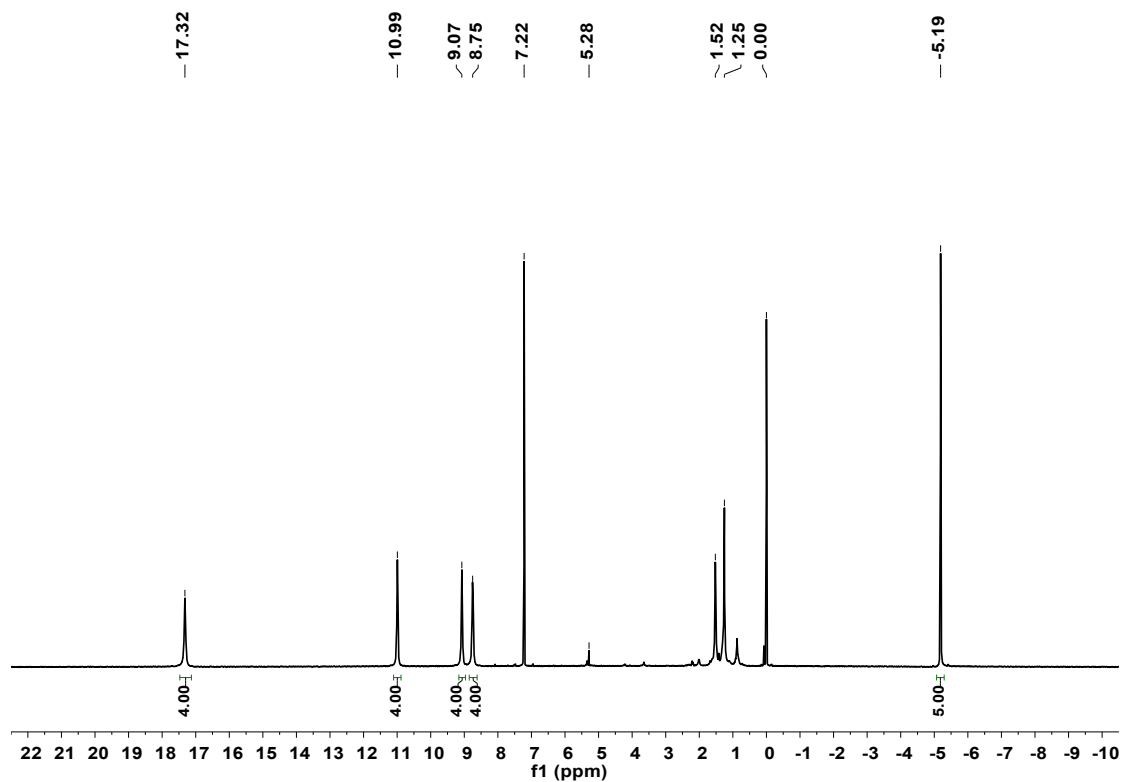


Figure S23. ^1H NMR (CDCl_3) of $[\text{D}_{18}]\text{-5-Yb}$

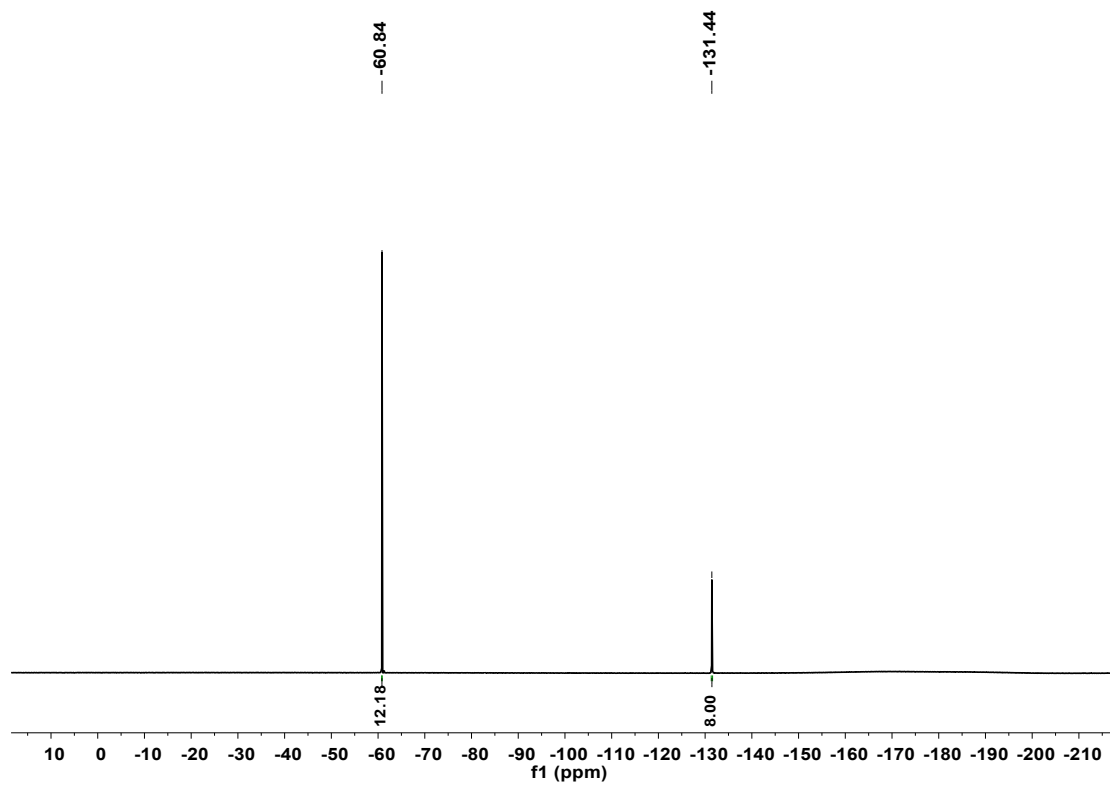


Figure S24. ^{19}F NMR (CDCl_3) of $[\text{D}_{18}]\text{-5-Yb}$

2.5 Experimental (up) and simulated (down) HR-ESI-MS spectra

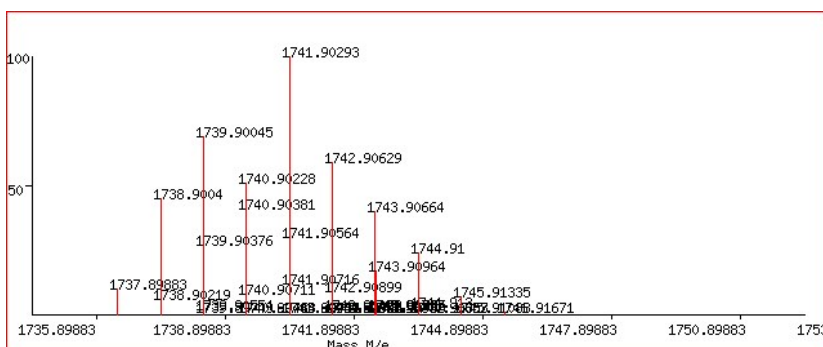
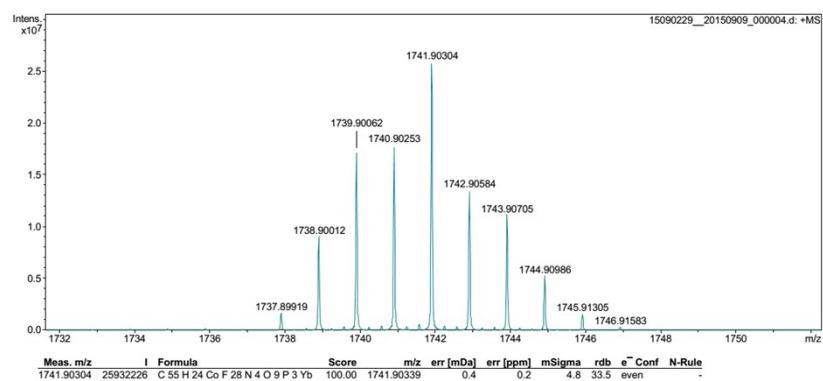


Figure S25. HR-ESI-MS spectrum of **1-Yb**

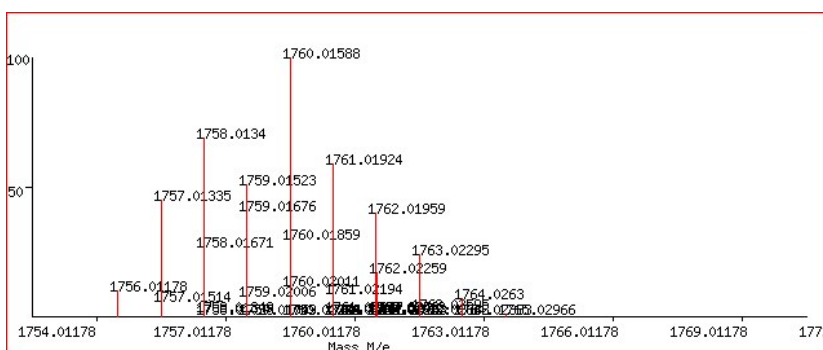
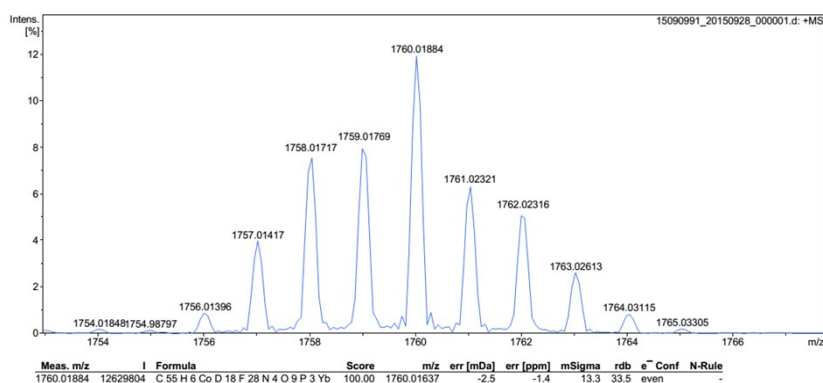


Figure S26. HR-ESI-MS spectrum of **[D₁₈]-1-Yb**

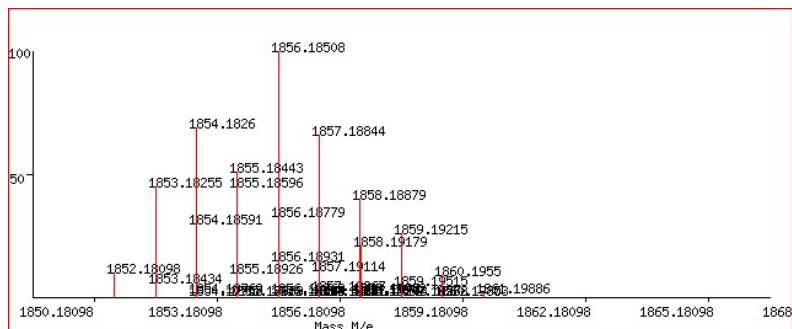
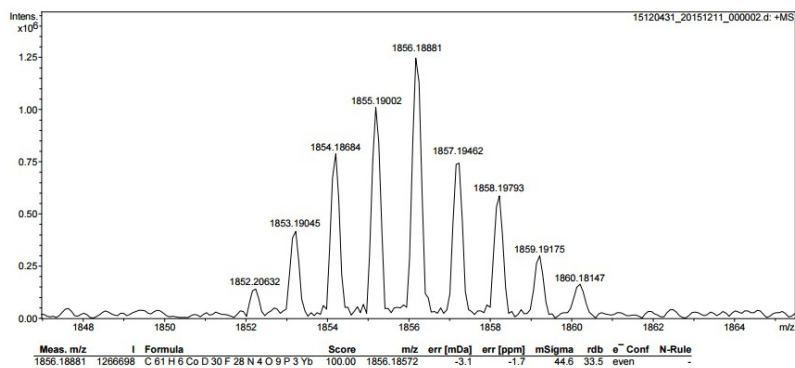


Figure S27. HR-ESI-MS spectrum of **[D₃₀]-1-Yb**

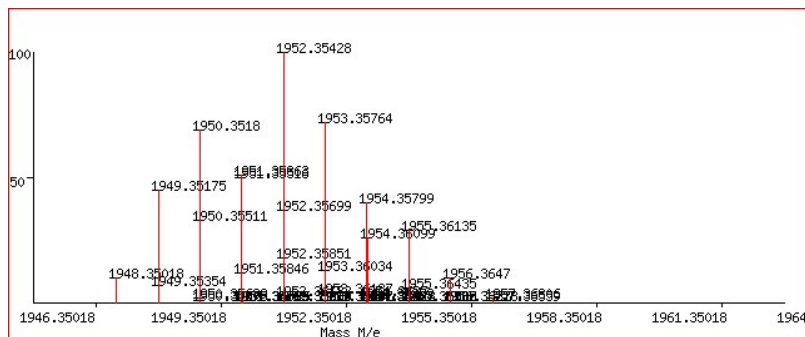
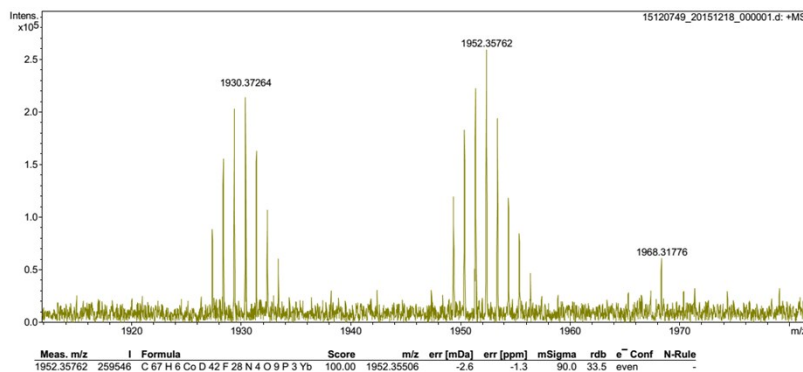


Figure S28. HR-ESI-MS spectrum of **[D₄₂]-1-Yb**

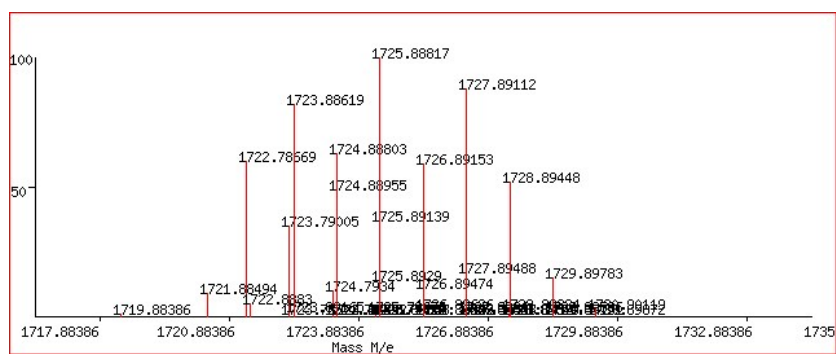
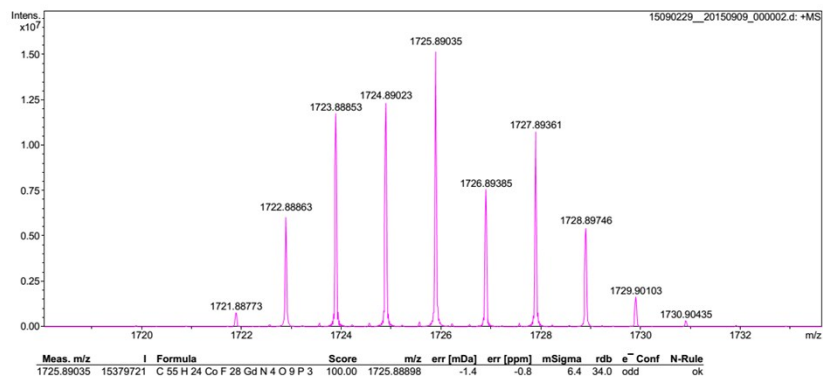


Figure S29. HR-ESI-MS spectrum **1-Gd**

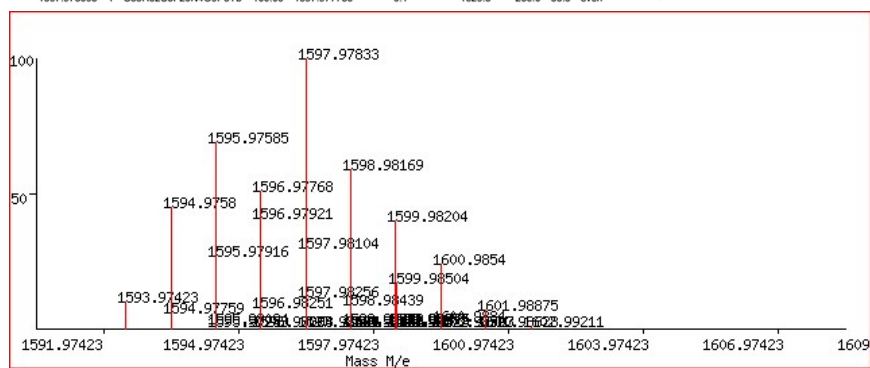
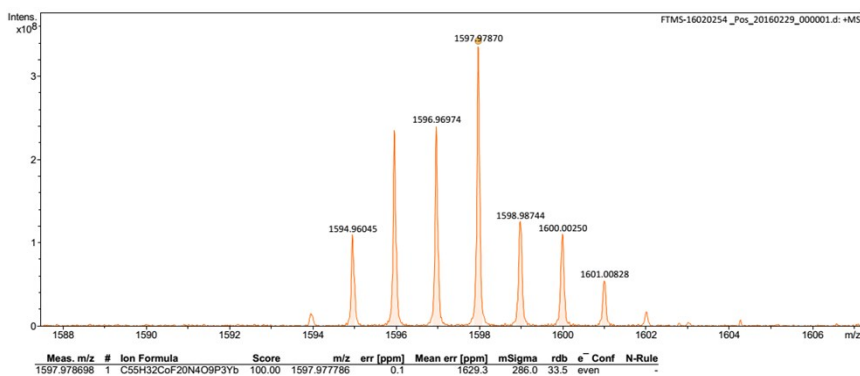


Figure S30. HR-ESI-MS spectrum of **2-Yb**

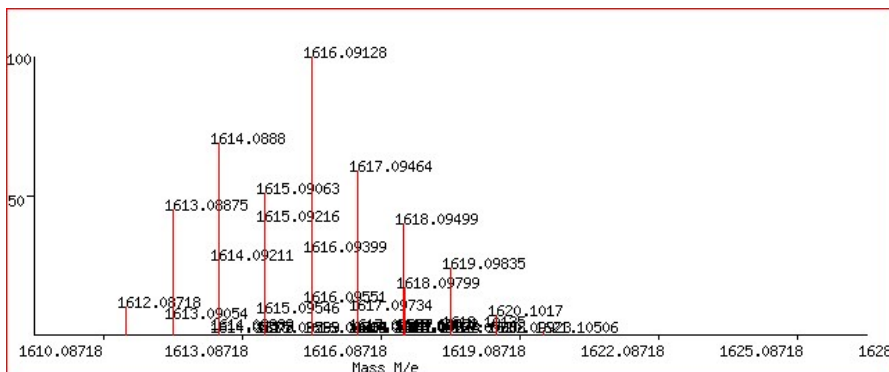
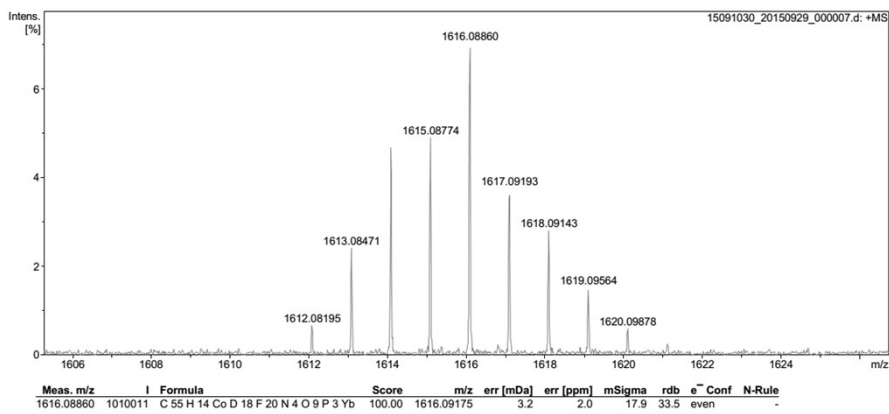


Figure S31. HR-ESI-MS spectrum of **[D₁₈]-2-Yb**

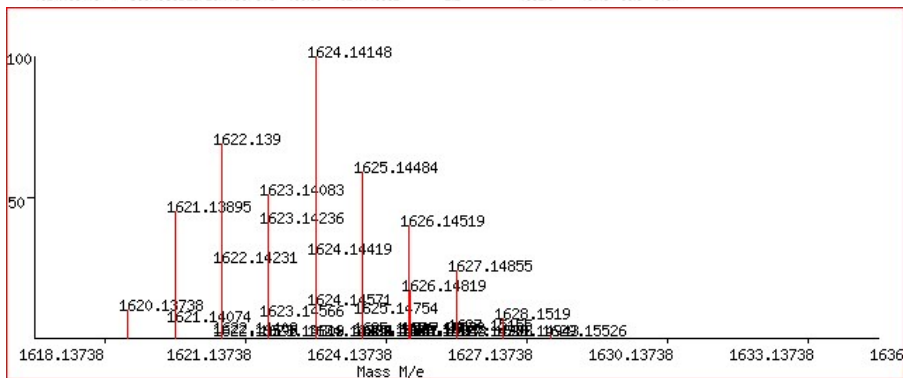
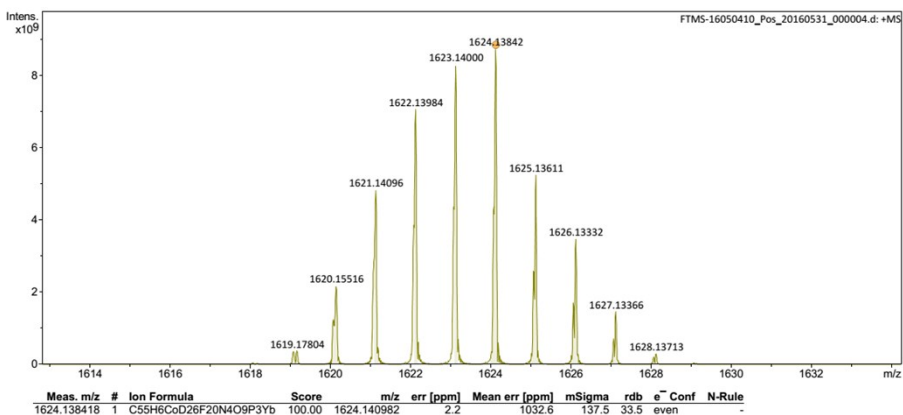


Figure S32. HR-ESI-MS spectrum of **[D₂₆]-2-Yb**

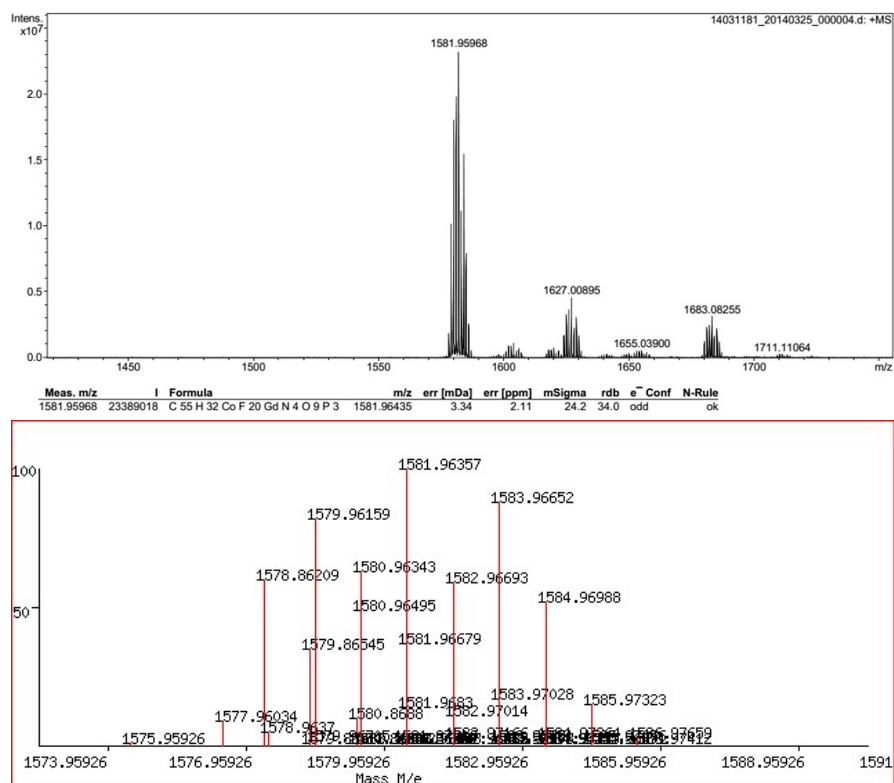


Figure S33. HR-ESI-MS spectrum of **2-Gd**

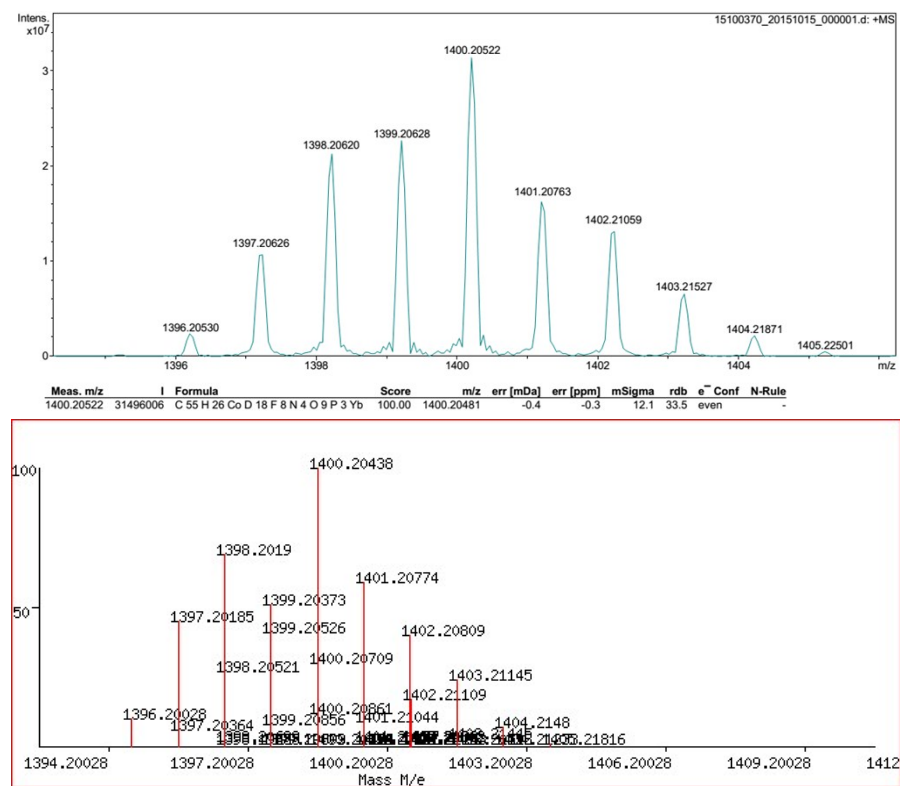


Figure S34. HR-ESI-MS spectrum of **[D₁₈]-3-Yb**

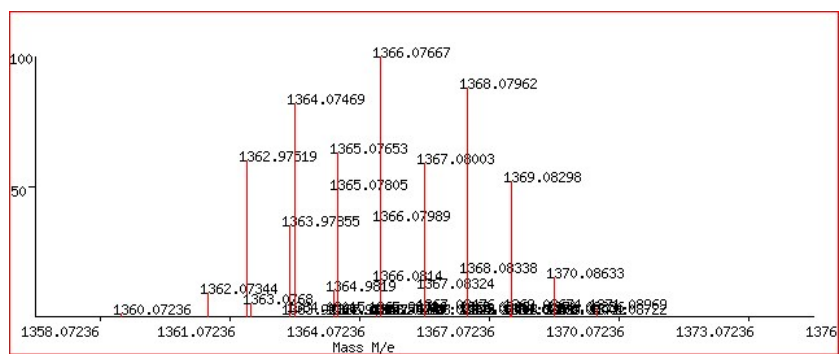
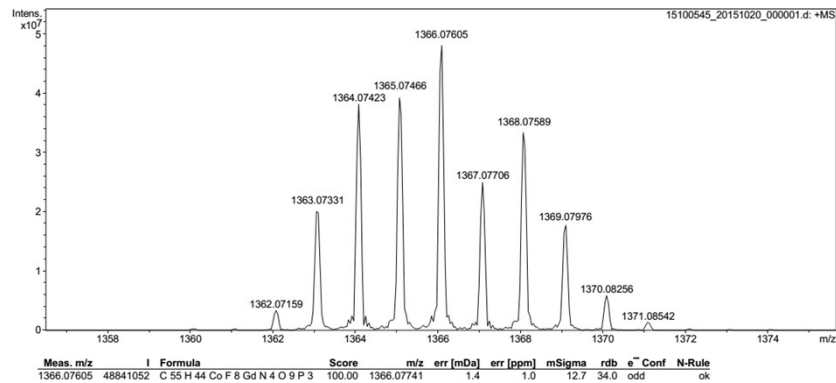


Figure S35. HR-ESI-MS spectrum of **3-Gd**

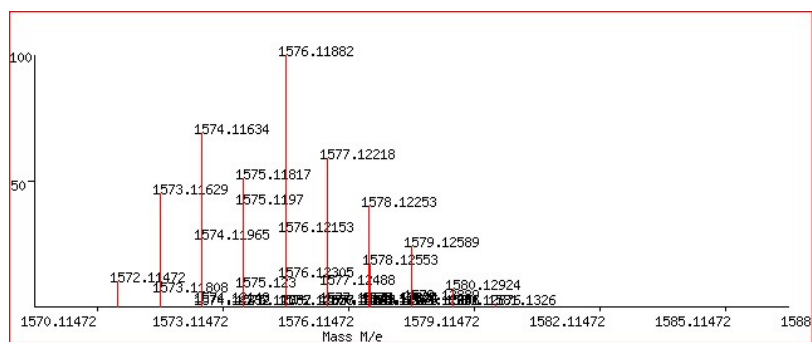
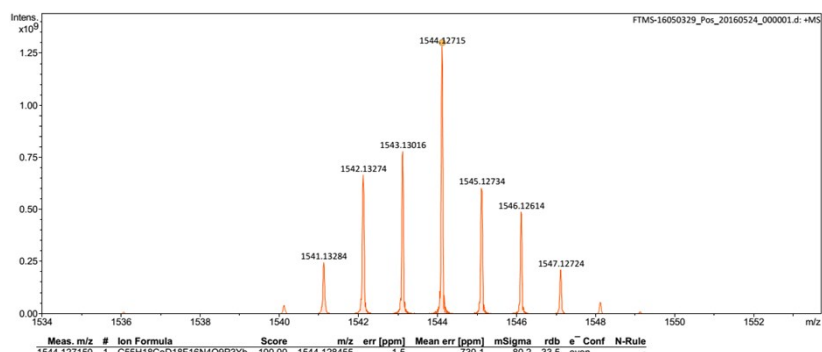


Figure S36. HR-ESI-MS spectrum of **[D₁₈]-4-Yb**

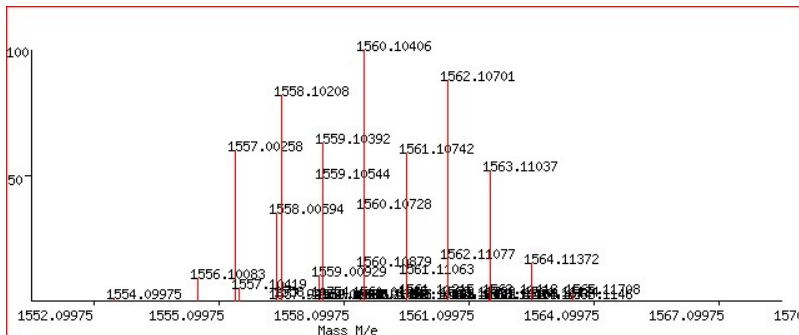
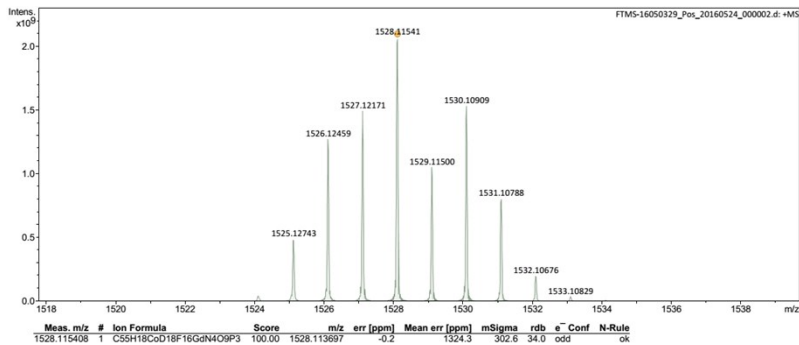


Figure S37. HR-ESI-MS spectrum of **[D₁₈]-4-Gd**

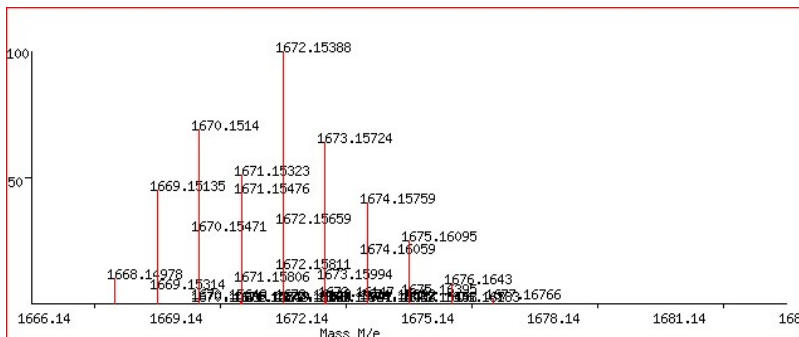
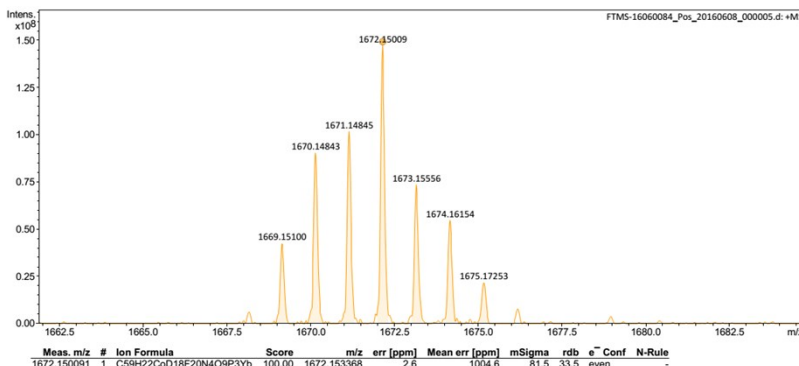


Figure S38. HR-ESI-MS spectrum of **[D₁₈]-5-Yb**

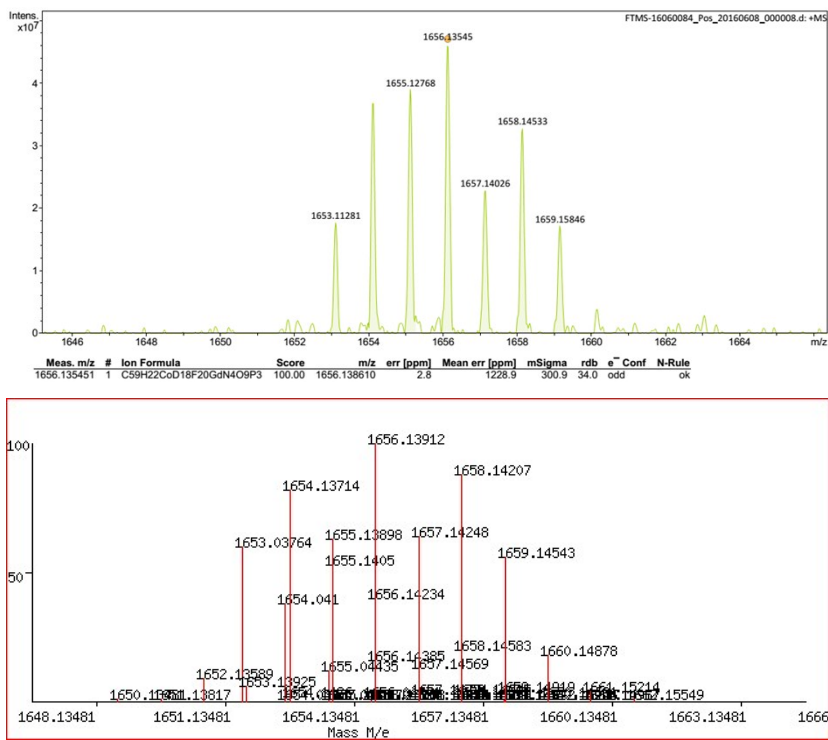


Figure S39. HR-ESI-MS spectrum of [D₁₈]-5-Gd

2.6 IR spectra.

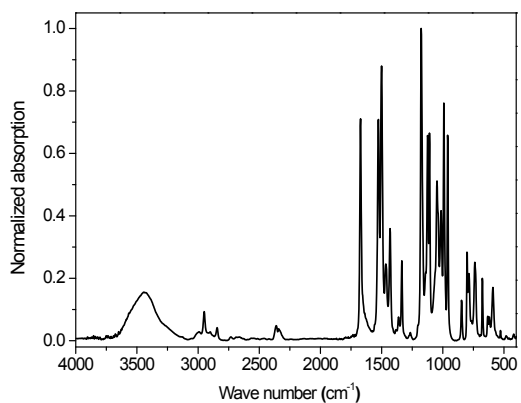


Figure S40. IR spectrum of **1-Yb**

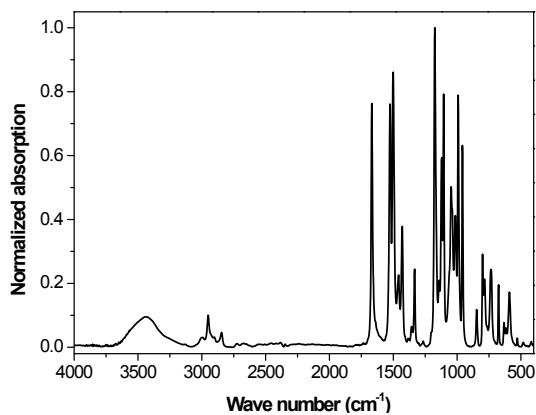


Figure S41. IR spectrum of **[D₁₈]-1-Yb**

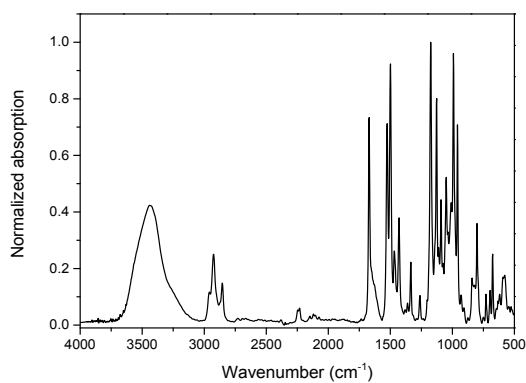


Figure S42. IR spectrum of **[D₃₀]-1-Yb**

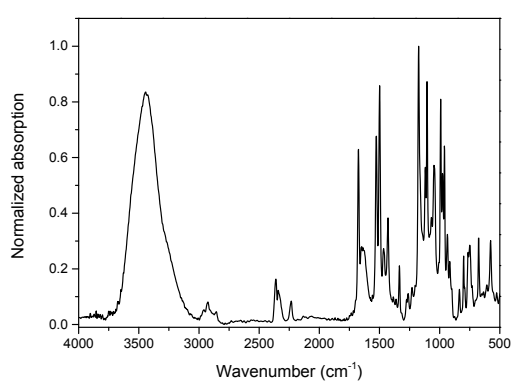


Figure S43. IR spectrum of **[D₄₂]-1-Yb**

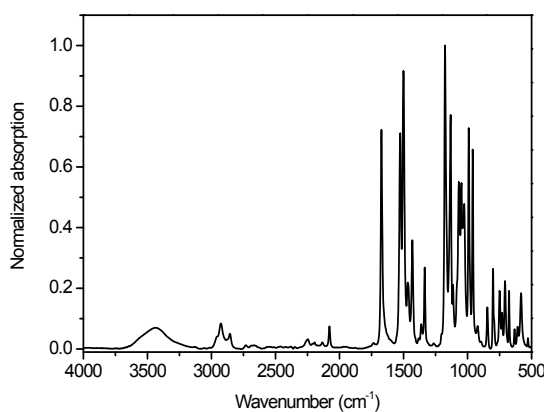


Figure S44. IR spectrum of **1-Gd**

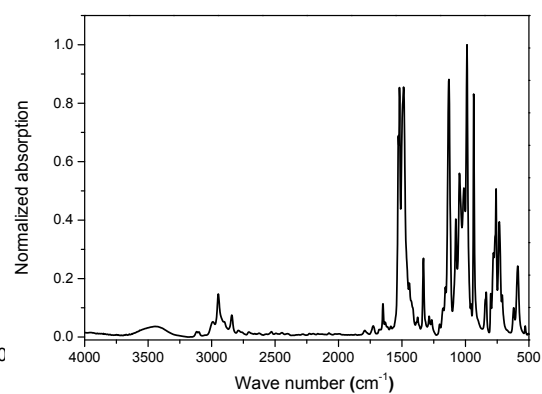


Figure S45. IR spectrum of **2-Yb**

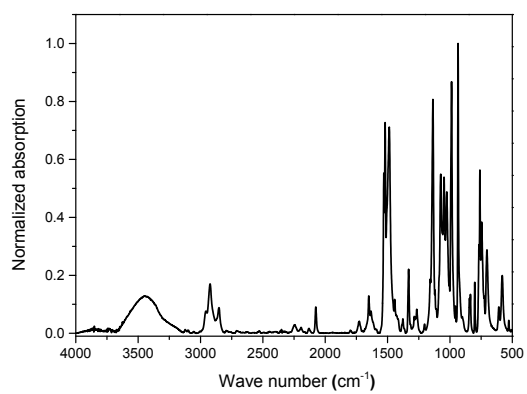


Figure S46. IR spectrum of **[D₁₈]-2-Yb**

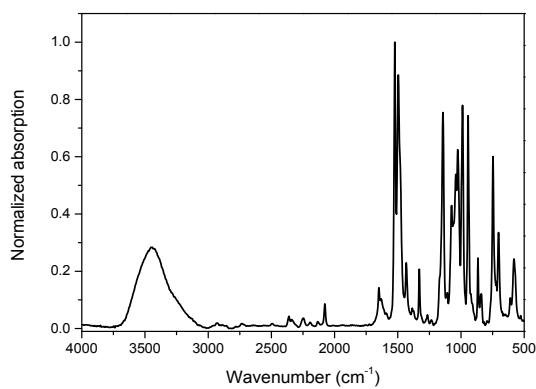


Figure S47. IR spectrum of **[D₂₆]-2-Yb**

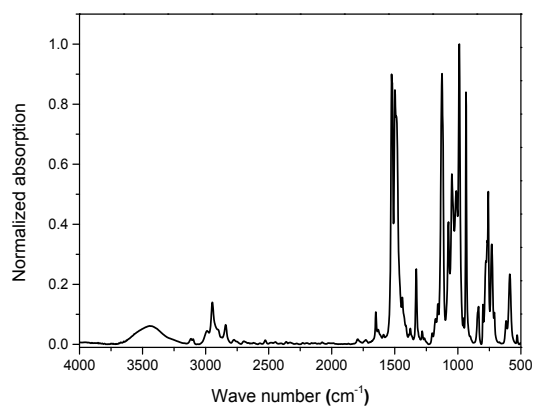


Figure S48. IR spectrum of **2-Gd**

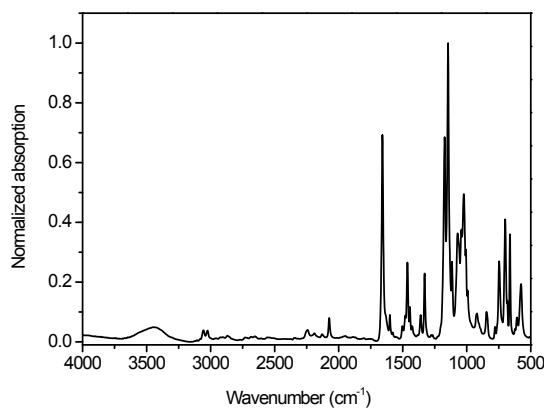


Figure S49. IR spectrum of **[D₁₈]-3-Yb**

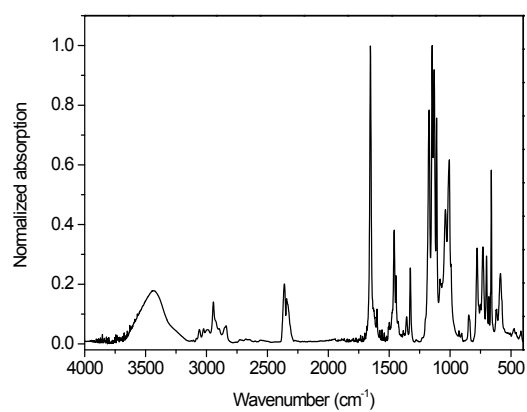


Figure S50. IR spectrum of **3-Gd**

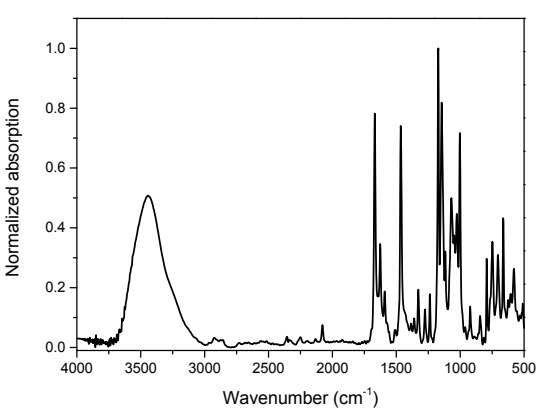


Figure S51. IR spectrum of **[D₁₈]-4-Yb**

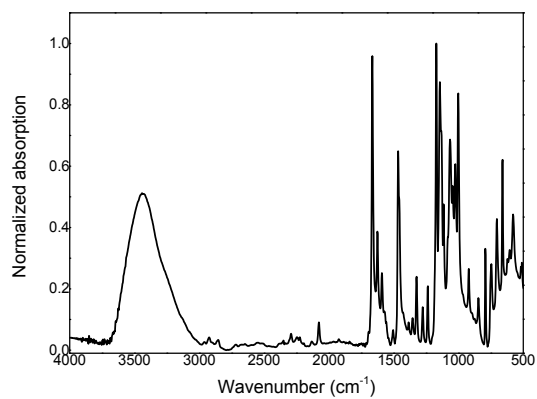


Figure S52. IR spectrum of **[D₁₈]-4-Gd**

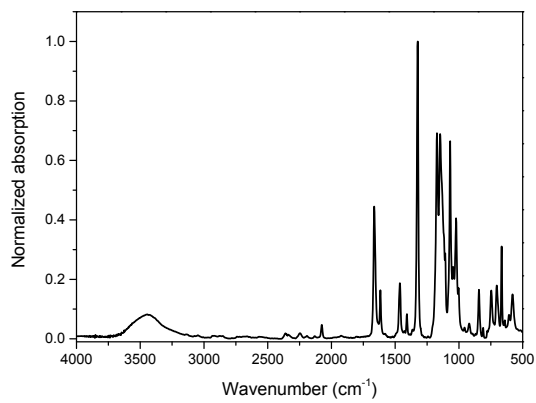


Figure S53. IR spectrum of **[D₁₈]-5-Yb**

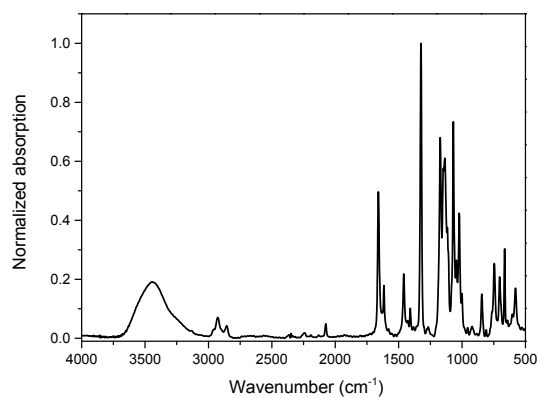


Figure S54. IR spectrum of **[D₁₈]-5-Gd**

3. Photophysical properties

3.1 General

Emission and excitation spectra were measured on an Edinburgh Analytical Instruments FLS920 lifetime and steady state spectrometer equipped with a 450w Xe lamp, a 5w microsecond flash lamp, a visible photomultiplier tube (PMT) detector (200–870 nm, R928P; Hamamatsu), and a NIR PMT detector (800–1700 nm, R5509–73 with C9940–02 cooler, Hamamatsu). Excitation and emission spectra were corrected for instrumental functions. Low temperature spectra were recorded on frozen glasses of solutions of Gd complexes (MeOH/EtOH 1:1, v/v) using a dewar cuvette filled with liquid N₂ (T = 77 K). NIR Quantum yields in CH₂Cl₂ and CD₂Cl₂ were measured by the optically dilute method using Yb(TPP)(LOEt) as the standard after excitation at λ_{ex} = 425 nm (2.4%, CH₂Cl₂ solution) according to the following equation:

$$\Phi_s = \frac{k_s}{k_r} \times \left(\frac{n_s}{n_r}\right)^2 \times \Phi_r$$

Where the subscripts *r* and *s* denote reference and sample respectively, Φ is the quantum yield, *k* is the slope from the plot of integrated emission intensity vs absorbance, and *n* is the refractive index of the solvent. The estimated error of quantum yield measurement is 15%.

The absolute quantum yield of **[D₁₈]-1-Yb** was determined in an integrating sphere on a FLS-920 (150 mm in diameter with the inner surface coated with PTFE to enable efficient scattering of light) according to the following equation:

$$\Phi = \frac{A_{em}}{(A_{scatter}^{ref} - A_{scatter}^{sample}) \times k_{Red/NIR}}$$

where *A_{em}* is the integrated area of the sample's emission (corrected); *A_{scatter}^{ref}* and *A_{scatter}^{sample}* are the integrated area under the Rayleigh scattering peaks of the reference sample and the sample under study; and *k_{Red/NIR}* is the ratio between sensitivities of two detectors, which was determined right after the measurement.

The quantum yields of **[D₁₈]-1-Yb** were also re-determined on a Horiba-Jobin-Yvon Fluorolog-3 spectrofluorimeter equipped with a iHR320 Imaging Spectrometer, a CCD detector (1024× 256 pixel, 200-1100 nm) and a Quanta-φ integrating sphere (150 mm, PTFE inner sphere) referenced to Yb(TPP)(LOEt).

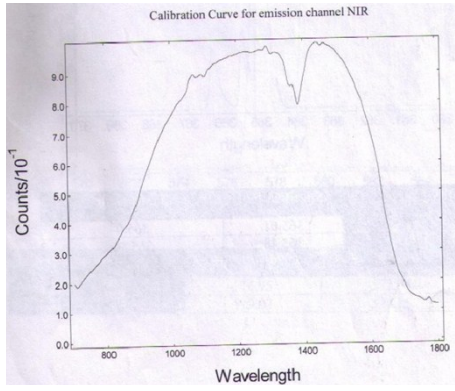


Figure S55. Calibration curve for NIR emission detector.

3.2 Absorption, excitation and steady-state emission spectra

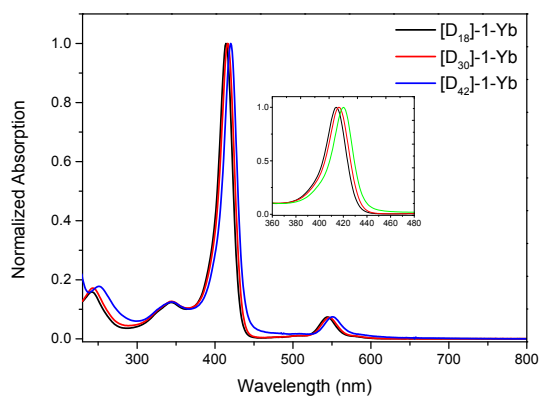


Figure S56. Normalized UV-vis absorption spectra of $[D_{18}]-1-Yb$, $[D_{30}]-1-Yb$ and $[D_{42}]-1-Yb$ in CH_2Cl_2 .

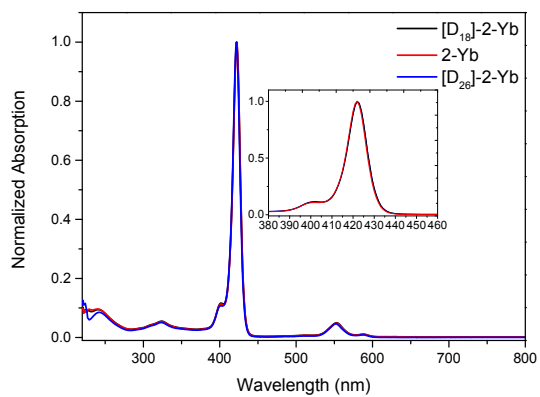


Figure S57. Normalized UV-vis absorption spectra of $2-Yb$, $[D_{18}]-2-Yb$, and $[D_{26}]-2-Yb$ in CH_2Cl_2 .

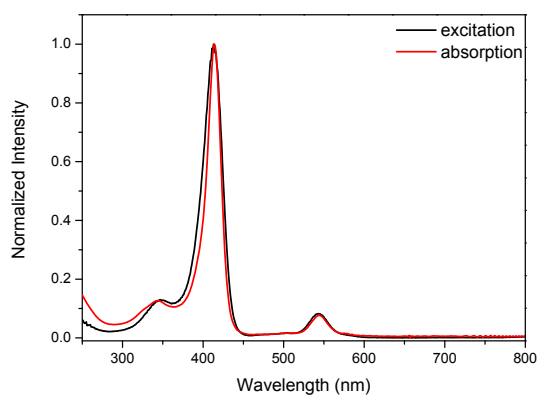


Figure S58 Normalized excitation absorption spectra of $1-Yb$ in CH_2Cl_2 monitored at 975 nm.

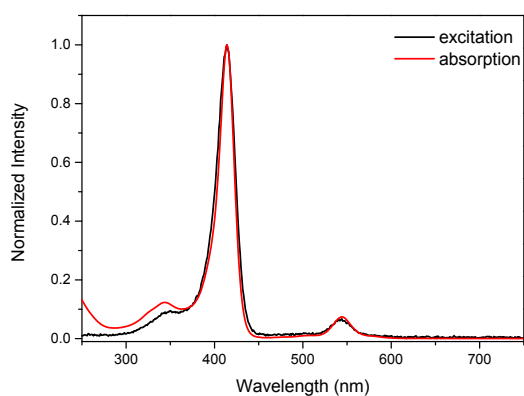


Figure S59 Normalized excitation absorption spectra of **[D₁₈]-1-Yb** in CH₂Cl₂ monitored at 975 nm.

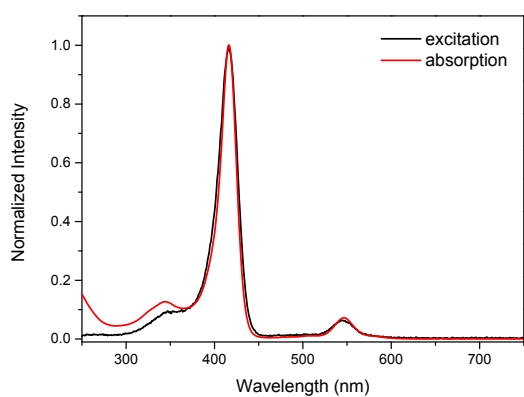


Figure S60 Normalized excitation absorption spectra of **[D₃₀]-1-Yb** in CH₂Cl₂ monitored at 975 nm.

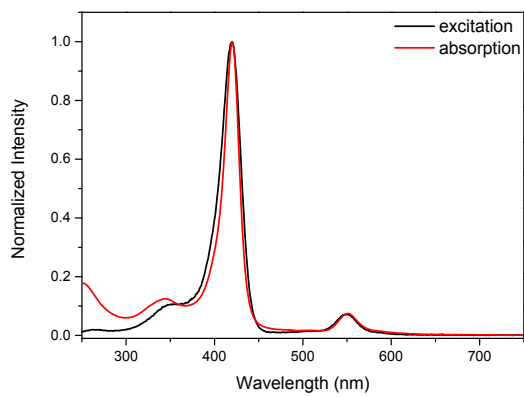


Figure S61 Normalized excitation absorption spectra of **[D₄₂]-1-Yb** in CH₂Cl₂ monitored at 975 nm.

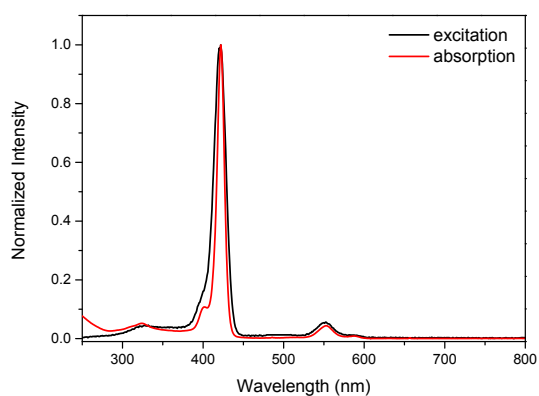


Figure S62 Normalized excitation absorption spectra of **2-Yb** in CH₂Cl₂ monitored at 975 nm.

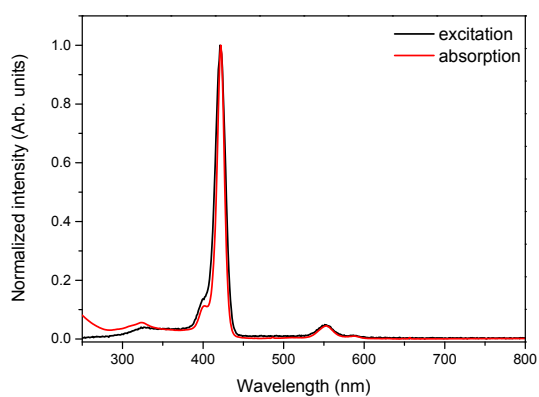


Figure S63 Normalized excitation absorption spectra of **[D₁₈]-2-Yb** in CH₂Cl₂ monitored at 975 nm.

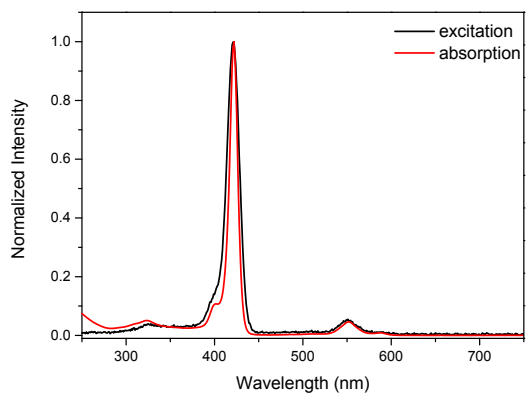


Figure S64 Normalized excitation absorption spectra of **[D₂₆]-2-Yb** in CH₂Cl₂ monitored at 975 nm.

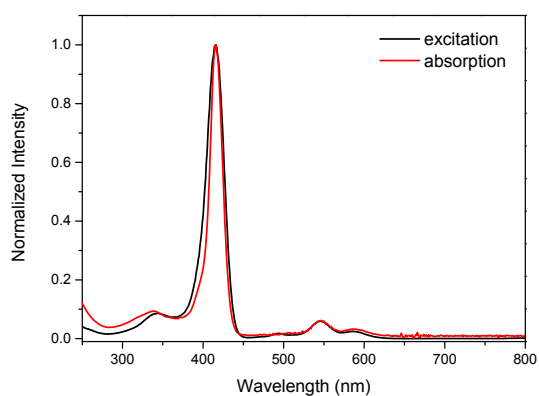


Figure S65 Normalized excitation absorption spectra of [D₁₈]-3-Yb in CH₂Cl₂ monitored at 975 nm.

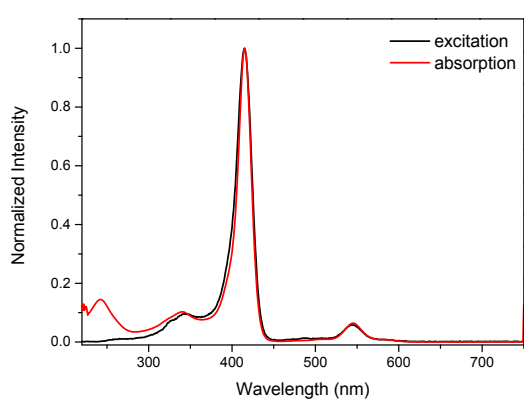


Figure S66 Normalized excitation absorption spectra of [D₁₈]-4-Yb in CH₂Cl₂ monitored at 975 nm.

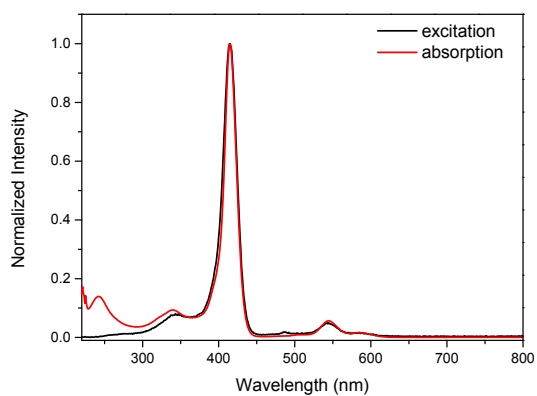


Figure S67 Normalized excitation absorption spectra of [D₁₈]-5-Yb in CH₂Cl₂ monitored at 975 nm.

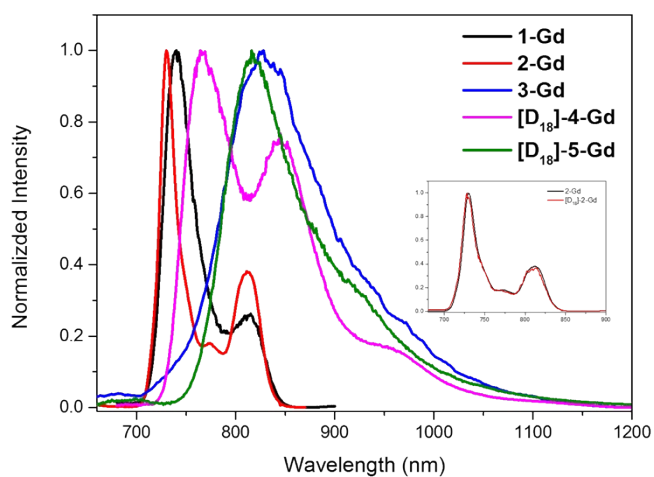


Figure S68. Low-temperature (77 K) steady state emission spectra for the transition T1→S0 of Gd(III) complexes in MeOH/EtOH (1:1, v/v). (Deuteration of Klau ligand does not affect the emission band of the Gd complex as shown in the inset.)

3.3 Luminescence decay profiles

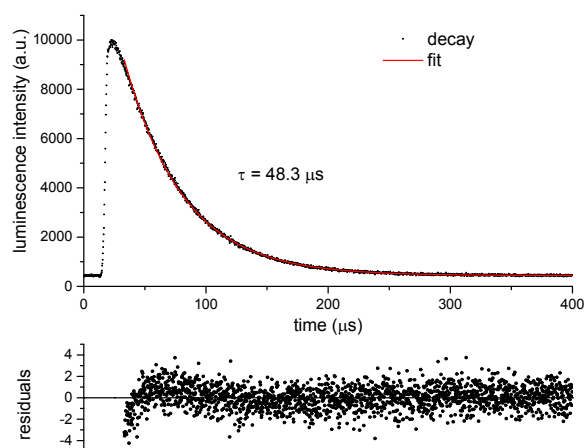


Figure S69. Luminescence decay profile of the transition ${}^2F_{5/2} \rightarrow {}^2F_{7/2}$ in **1-Yb** in CH_2Cl_2 .

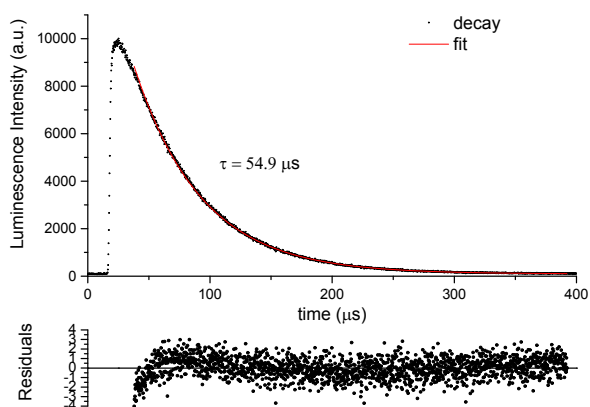


Figure S70. Luminescence decay profile of the transition ${}^2F_{5/2} \rightarrow {}^2F_{7/2}$ in **1-Yb** in CD_2Cl_2 .

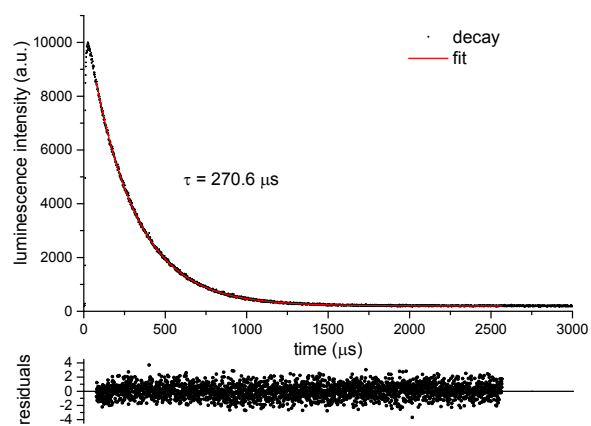


Figure S71. Luminescence decay profile of the transition ${}^2F_{5/2} \rightarrow {}^2F_{7/2}$ in **[D₁₈]-1-Yb** in CH_2Cl_2 .

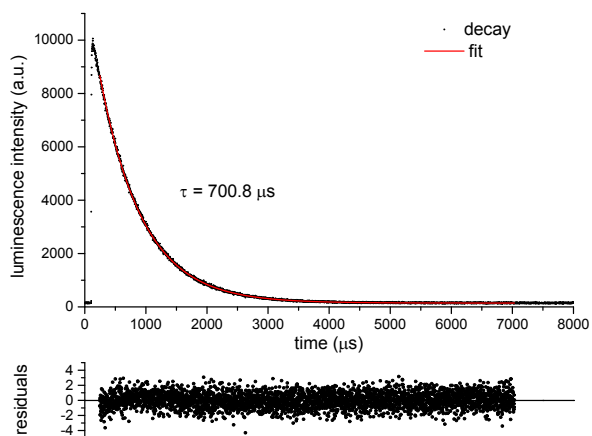


Figure S72. Luminescence decay profile of the transition ${}^2F_{5/2} \rightarrow {}^2F_{7/2}$ in $[\mathbf{D}_{18}]\text{-1-Yb}$ in CD_2Cl_2 .

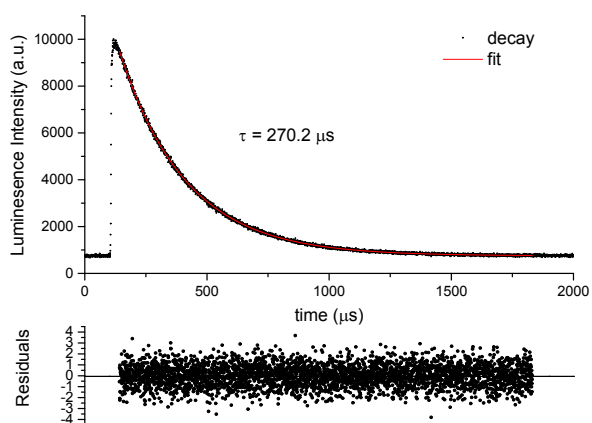


Figure S73. Luminescence decay profile of the transition ${}^2F_{5/2} \rightarrow {}^2F_{7/2}$ in $[\mathbf{D}_{30}]\text{-1-Yb}$ in CH_2Cl_2 .

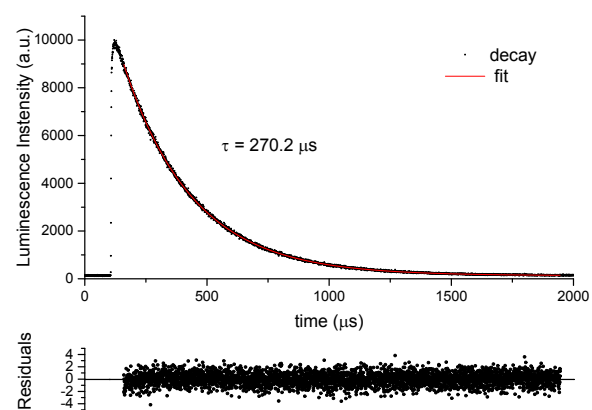


Figure S74. Luminescence decay profile of the transition ${}^2F_{5/2} \rightarrow {}^2F_{7/2}$ in $[\mathbf{D}_{42}]\text{-1-Yb}$ in CH_2Cl_2 .

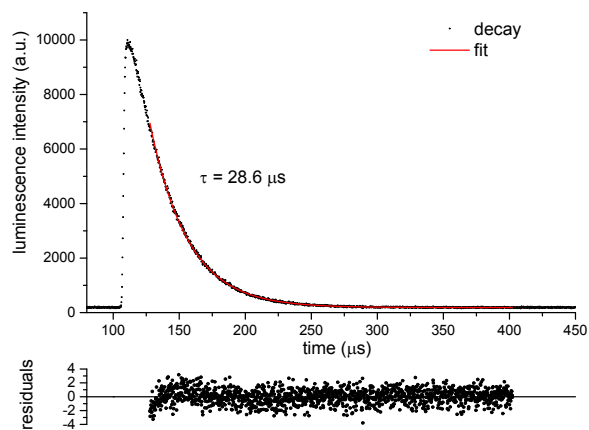


Figure S75. Luminescence decay profile of the transition ${}^2F_{5/2} \rightarrow {}^2F_{7/2}$ in **2-Yb** in CH_2Cl_2 .

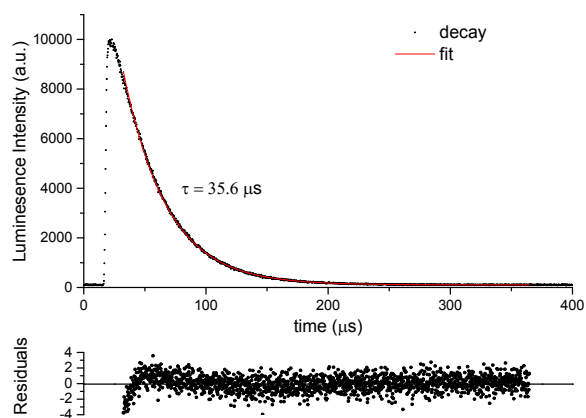


Figure S76. Luminescence decay profile of the transition ${}^2F_{5/2} \rightarrow {}^2F_{7/2}$ in **2-Yb** in CD_2Cl_2 .

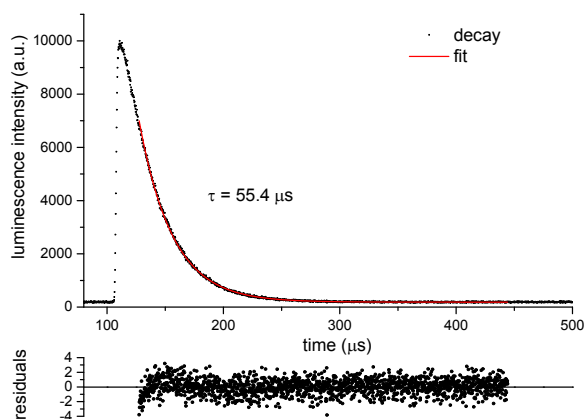


Figure S77. Luminescence decay profile of the transition ${}^2F_{5/2} \rightarrow {}^2F_{7/2}$ in **[D₁₈]-2-Yb** in CH_2Cl_2 .

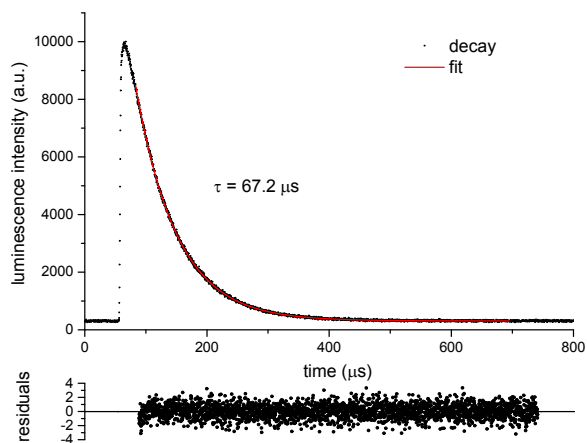


Figure S78. Luminescence decay profile of the transition ${}^2F_{5/2} \rightarrow {}^2F_{7/2}$ in **[D₁₈]-2-Yb** in CD_2Cl_2 .

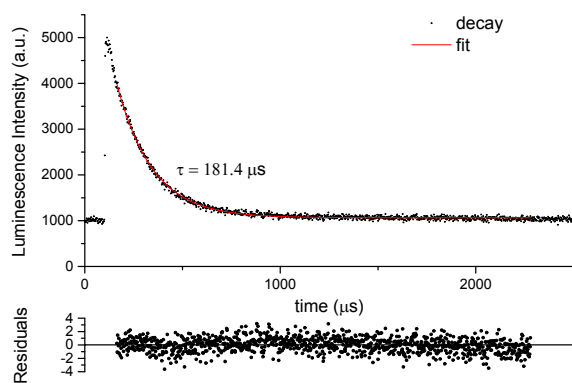


Figure S79. Luminescence decay profile of the transition ${}^2F_{5/2} \rightarrow {}^2F_{7/2}$ in **[D₂₆]-2-Yb** in CH_2Cl_2 .

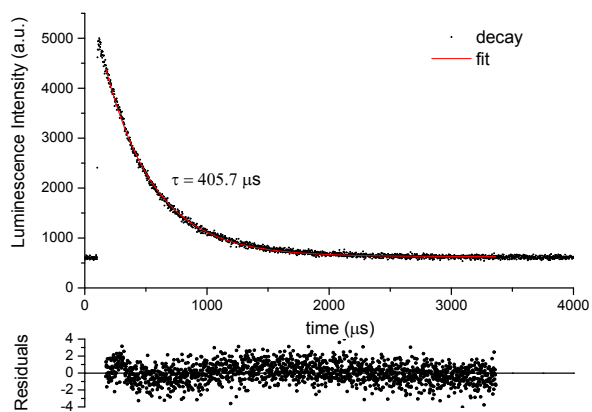


Figure S80. Luminescence decay profile of the transition ${}^2F_{5/2} \rightarrow {}^2F_{7/2}$ in **[D₂₆]-2-Yb** in CD_2Cl_2 .

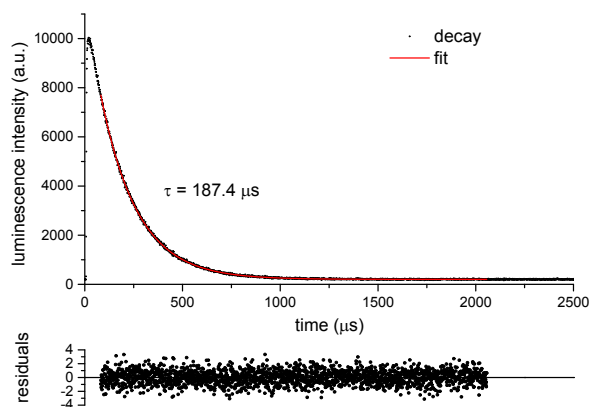


Figure S81. Luminescence decay profile of the transition ${}^2F_{5/2} \rightarrow {}^2F_{7/2}$ in **[D₁₈]-3-Yb** in CH₂Cl₂.

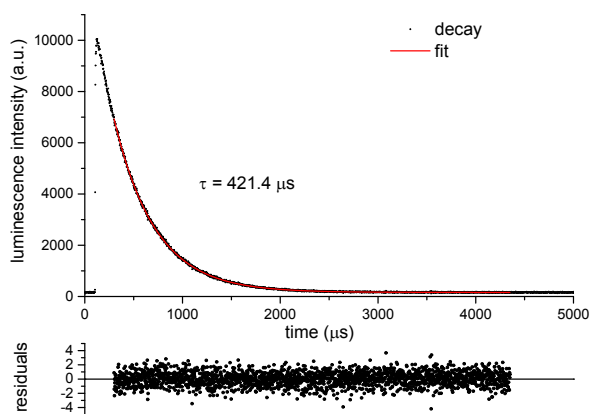


Figure S82. Luminescence decay profile of the transition ${}^2F_{5/2} \rightarrow {}^2F_{7/2}$ in **[D₁₈]-3-Yb** in CD₂Cl₂.

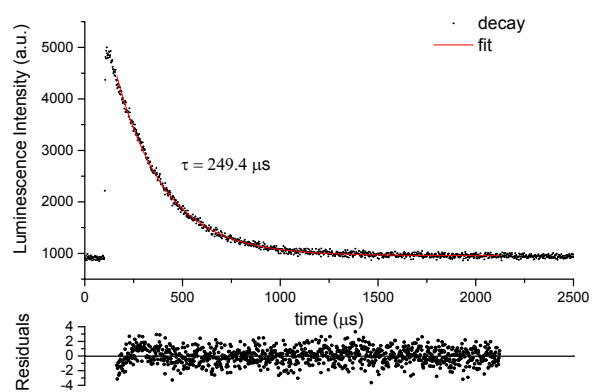


Figure S83. Luminescence decay profile of the transition ${}^2F_{5/2} \rightarrow {}^2F_{7/2}$ in **[D₁₈]-4-Yb** in CH₂Cl₂.

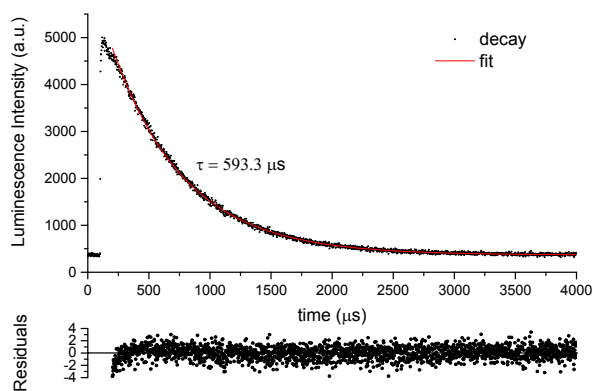


Figure S84. Luminescence decay profile of the transition ${}^2F_{5/2} \rightarrow {}^2F_{7/2}$ in **[D₁₈]-4-Yb** in CD_2Cl_2 .

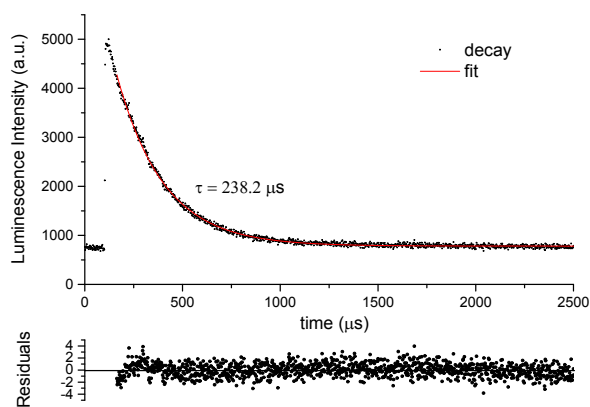


Figure S85. Luminescence decay profile of the transition ${}^2F_{5/2} \rightarrow {}^2F_{7/2}$ in **[D₁₈]-5-Yb** in CH_2Cl_2 .

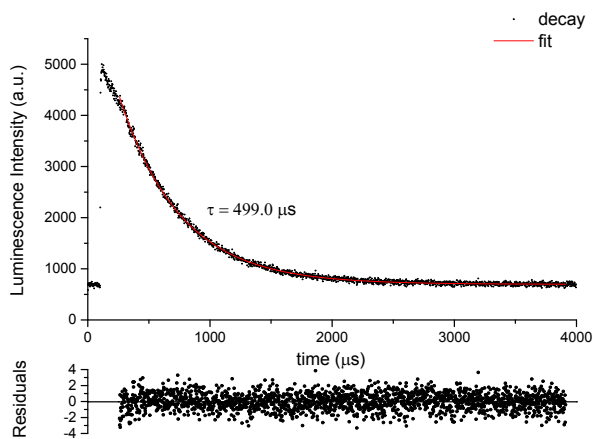
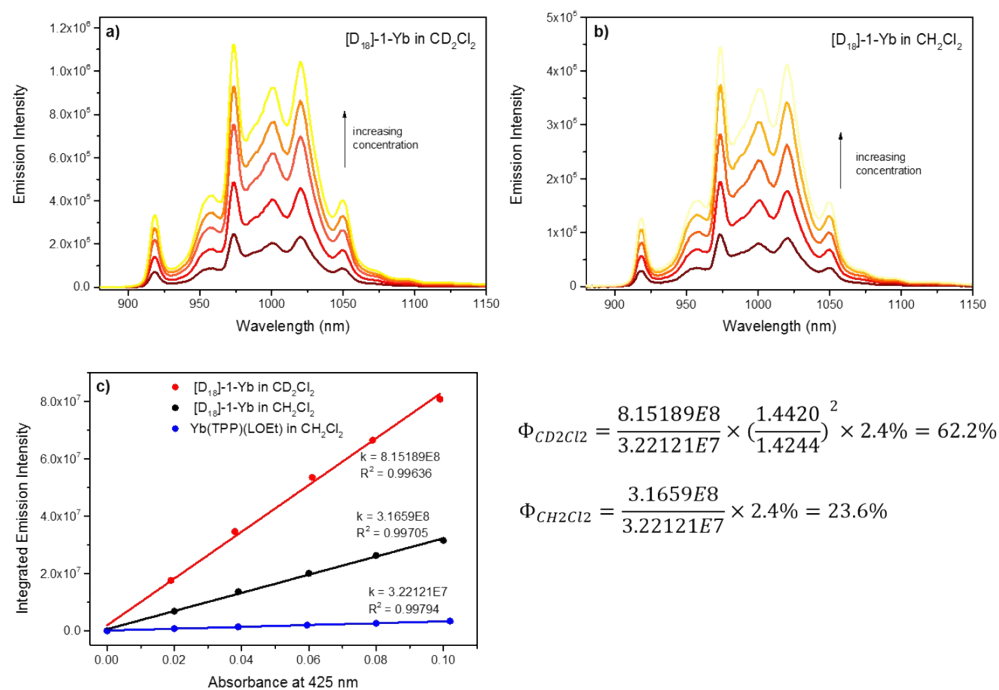


Figure S86. Luminescence decay profile of the transition ${}^2F_{5/2} \rightarrow {}^2F_{7/2}$ in **[D₁₈]-5-Yb** in CD_2Cl_2 .

3.4 NIR quantum yield measurement

3.4.1 Results *via* FLS 920 - Comparative Method



$$\Phi_{CD_2Cl_2} = \frac{8.15189E8}{3.22121E7} \times \left(\frac{1.4420}{1.4244}\right)^2 \times 2.4\% = 62.2\%$$

$$\Phi_{CH_2Cl_2} = \frac{3.1659E8}{3.22121E7} \times 2.4\% = 23.6\%$$

Figure S87. The emission spectra of complex $[D_{18}]$ -1-Yb in CD_2Cl_2 (a) and CH_2Cl_2 (b) and plot (emission vs absorbance, c) for the emission quantum yield determination.

3.4.2 Results via FLS 920 – Integrating Sphere



Figure S88. The absolute QY measurement of **[D₁₈]-1-Yb** in CH₂Cl₂ ($\lambda_{\text{ex}} = 414 \text{ nm}$).

$$\Phi = \frac{0.34\%}{0.0127} = 26\% (k_{\text{Red/NIR}} = 0.0127)$$

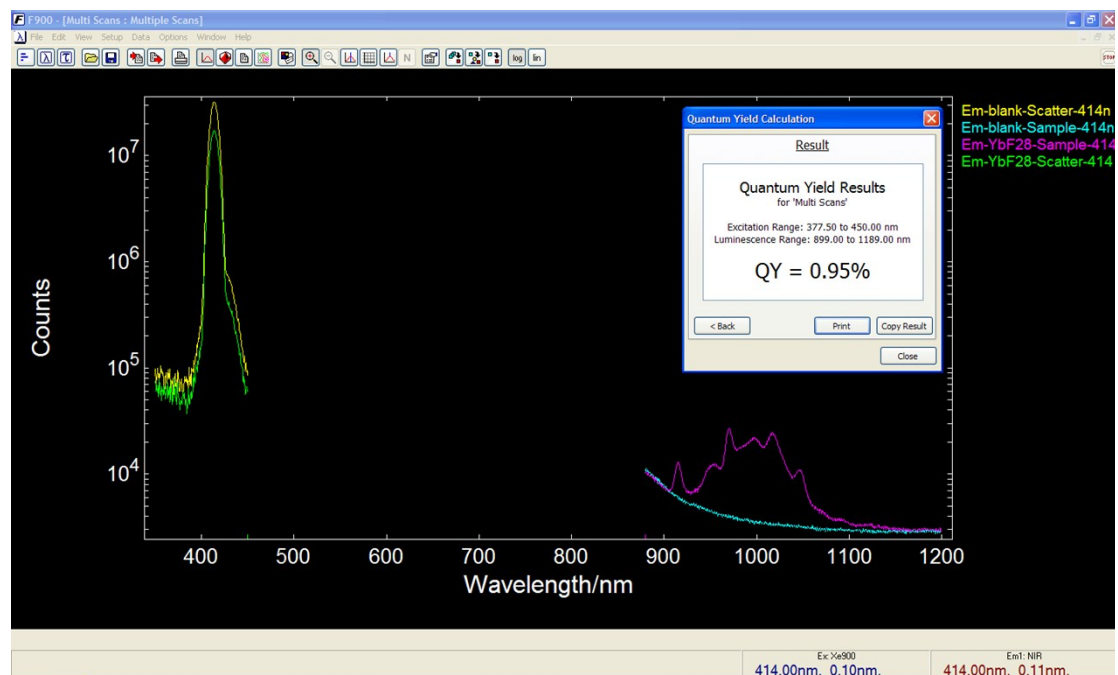


Figure S89. The absolute QY measurement of **[D₁₈]-1-Yb** in CD₂Cl₂ ($\lambda_{\text{ex}} = 414 \text{ nm}$).

$$\Phi = \frac{0.95\%}{0.0136} = 69\% (k_{\text{Red/NIR}} = 0.0136)$$

3.4.3 Results via Fluorolog-3 spectrofluorimeter

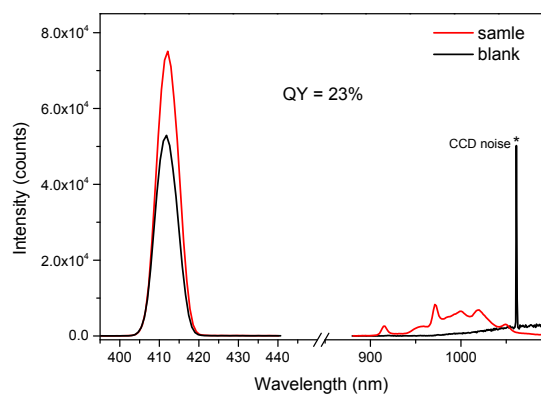


Figure S90. Quantum yield measurement of **[D₁₈]-1-Yb** in CH₂Cl₂ ($\lambda_{\text{ex}} = 414$ nm)

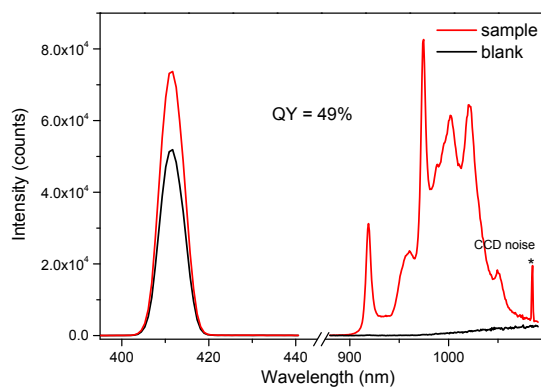


Figure S91. Quantum yield measurement of **[D₁₈]-1-Yb** in CD₂Cl₂ ($\lambda_{\text{ex}} = 414$ nm)

3.5 Calculation of the quenching rate difference Δk

The quenching rate difference Δk between C-(H/D) or C-(H/F) were calculated according to the following equation. The average value of Δk was given assuming that Δk of a specific site is not influenced by one another.

$$\Delta k = k_{D/F} - k_H = \left(\frac{1}{\tau_{D/F}} - \frac{1}{\tau_H} \right)$$

Table S3. Quenching rate differences Δk (in ms^{-1}) for individual C-(H/D) or C-(H/F) on different sites

	Compounds used to calculate	Average Δk / ms^{-1}
Kläui ligand	1-Yb vs. [D₁₈]-1-Yb 2-Yb vs. [D₁₈]-2-Yb	16.1
β pyrrolic	$\Delta k_{F/H}$: 1-Yb vs. 2-Yb [D₁₈]-1-Yb vs. [D₁₈]-2-Yb	13.5
	$\Delta k_{D/H}$: [D₂₆]-2-Yb vs. [D₁₈]-2-Yb	12.8
	$\Delta k_{F/D}$: [D₂₆]-2-Yb vs. [D₁₈]-1-Yb	1.6
<i>o</i> -Ph	[D₁₈]-4-Yb vs. [D₁₈]-3-Yb	0.8
<i>m</i> - and <i>p</i> -Ph	[D₁₈]-1-Yb vs. [D₁₈]-4-Yb	0.4
solvent	CD ₂ Cl ₂ vs. CH ₂ Cl ₂ for all the complexes	2.6

3.6 Radiative luminescence lifetime τ_{rad} measurement

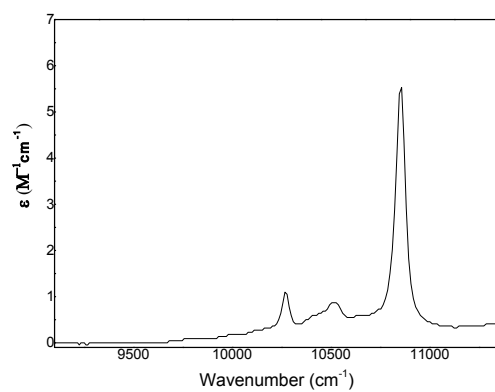


Figure S92. Quantitative absorption spectra of the f-f transitions in **[D₁₈]-3-Yb** ($c = 22.4$ mM) in CD_2Cl_2 .

4. References

- 1 Woller, E. K. & DiMugno, S. G. 2,3,7,8,12,13,17,18-Octafluoro-5,10,15,20-tetraarylporphyrins and Their Zinc Complexes: First Spectroscopic, Electrochemical, and Structural Characterization of a Perfluorinated Tetraarylmetalloporphyrin. *J. Org. Chem.* **62**, 1588-1593 (1997).
- 2 Allen, K. J. H. *et al.* Lanthanide Complexes of the Kläui Metalloligand, CpCo(P=O(OR)₂)₃: An Examination of Ligand Exchange Kinetics between Isotopomers by Electrospray Mass Spectrometry. *Inorg. Chem.* **51**, 12436-12443 (2012).
- 3 Wong, C.-P., Venteicher, R. F. & Horrocks Jr, W. D. Lanthanide porphyrin complexes. Potential new class of nuclear magnetic resonance dipolar probe. *J. Am. Chem. Soc.* **96**, 7149-7150 (1974).